UAlg FCT
UNIVERSIDADE DO ALGARVE
FACULDADE DE CIÊNCIAS E TECNOLOGIA

UNIVERSIDADE DO ALGARVE

Drug Repurposing in the Treatment of Melanoma Brain Metastasis

Billy Samuel Hill

Dissertação de Mestrado
Mestrado em Biologia Molecular e Microbiana

Trabalho efectuado sob a orientação de:

Professor Doutor Frits Thorsen
Professora Doutora Maria Leonor Cancela

2015

Declaração de Autoria de Trabalho

"Drug Repurposing in the Treatment of Melanoma Brain Metastasis"

Declaro ser o autor deste trabalho, que é original e inédito. Autores e trabalhos e consultados estão devidamente citados no texto e constam da listagem de referências incluída.

Assinatura: _____

Universidade do Algarve, 30 de Setembro 2015

Acknowledgements

First and foremost I would like to sincerely thank Professor Frits Thorsen, for accepting me, a student that he had never met and for allowing me to work on this really amazing project. There were good moments and not so good moments, but Professor Thorsen you helped me along every step of the way. To add to this a huge thank you for introducing me to this field of research. My most heart felt thanks.

I am also most grateful to Stian Krog, for all of his help in establishing the agreements and taking care of all the necessary paperwork, and having time to answer all my silly questions and doubts, Cheers Stian.

I would also like to thank all the staff and members at the MIC facility, Jebsen center and all the 6th floor lab personnel, for all the help and patience.

To all the researchers and students who used the same lab, big thanks for helping when I had problems or questions, for putting up with my loud music, and for all being great people to work with. I would like to give a special shout out to Nazanin Mola, the person I got to know the most, my right hand women, for all of what you did and helped me with, will never be forgotten, cheers sweetie.

I could not forget of course Birgitte de Martens, who was my little confidant, and was there in all the good and bad times ☺

I have to also thank my course committee, emphasizing Professor Filomena Fonseca, and my Co-coordinator Professor Leonor Cancela, for all the availability and help that they have provided throughout all this experience.

I am very grateful for all the support my best friend Renata Moreira gave me, a person who has always been there and always will be.

Also to all the people who kept in touch during the period of my absence, who kept me updated about all that's been going on, and for great conversations and support. Especially Margarida Castro.

And finally last but not least to my parents without whom this all would not have been possible, who have supported me no matter what, thank you for everything, lots of love.

Hasta la vista.

Resumo

O melanoma maligno é considerado a forma mais letal de cancro de pele, com uma elevada tendência para metastizar para o cérebro. Atualmente, as metástases cerebrais são tratadas através de cirurgia, quimioterapia, radioterapia e radiocirurgia, mas o sucesso destes tratamentos são mínimos, como tal novas estratégias terapêuticas são importantes e necessárias.

A fim de determinar novas estratégias de terapia cancerígena, são precisos modelos animais adequados para investigar os efeitos dos tratamentos. Em trabalhos anteriores, desenvolveu-se um novo modelo animal, através de injecção, na corrente sanguínea de organismos imunodeficientes (nod/scid), de células de melanoma humano . Estes animais imunodeficientes, para além de desenvolver tumores cerebrais, também desenvolveram metástases em outros órgãos. A partir dos tumores desenvolvidos, foi determinada, por sequenciamento de RNA, uma lista de genes candidatos responsáveis pelas metástases cerebrais,. Com uma análise bioinformática, utilizando o *connectivity map* (cMAP), foi possível encontrar várias drogas, administradas em pacientes para outros fins terapêuticos, que podem ser também eficazes no tratamento de metástases cerebrais.

O objetivo deste trabalho foi testar os fármacos candidatos, determinados pelas sequencias de RNA, em quatro linhas celulares diferentes de melanoma humano. Dos ensaios *in vitro* realizados com 9 drogas candidatas, apenas 5 mostraram ter algum potencial, mas só 3 foram selecionadas (Tricostatina A, Metildopa e Pentamidina) para serem testadas *in vivo*. Esta seleção baseou-se na análise do peso molecular, devido às limitações da passagem pela barreira hematoencefálica.

Nos resultados *in vivo*, observou-se um efeito positivo, ainda que transitório, sobre a carga tumoral e o volume do tumor após quatro semanas de tratamento, quando eram expostos com metildopa. Assim, estudos adicionais têm de ser realizados utilizando a metildopa, para se confirmar e validar os resultados obtidos, e perceber se é suficientemente eficaz para ser utilizada de forma preventiva.

Com este trabalho também foi possível otimizar-se protocolos de ressonância magnética para facilitar a observação dos tumores, especialmente os de menores dimensões. Para além disso, a ressonância magnética também permite verificar se os tumores estão a invadir tecidos circundantes. Este protocolo tornou-se uma boa ferramenta que pode ser usado em futuros

estudos, permitindo estudar de forma mais eficaz as alterações dos tumores, e contribuir assim para o desenvolvimento de melhores tratamentos.

Abstract

Malignant melanoma is the most lethal form of skin cancer, with a high propensity to metastasize to the brain. Melanoma brain metastases are currently treated with surgery, chemotherapy, radiotherapy and radiosurgery. Positive treatment results are, however minimal, and new therapeutic strategies are therefore needed.

In order to determine new treatment strategies, suitable animal models to study effects of treatment are crucial. In previous work done in the group, a novel animal model was developed, by injecting human melanoma brain metastasis cell lines into the blood stream of immunodeficient (nod/scid) mice, with subsequent metastasis to the animal organs. From these tumors, a candidate gene list responsible for melanoma brain metastasis was determined by RNA sequencing. Subsequent bioinformatics analysis using Connectivity Map was used to find several drugs already used on patients for other purposes than cancer, which may also be effective in the treatment of melanoma brain metastasis.

The aim of this work was to test the identified potential new drug candidates, on melanoma metastatic cell lines. In the first part of the work, *in vitro* assays were performed to investigate the potential effects of nine of the drug candidates on four different human melanoma metastatic cell lines. From these 9 candidates 5 showed potential and three were selected for *in vivo* studies (Trichostatin A, Methyldopa and Pentamidine). Only these were selected due to molecular weight and limitations of the blood brain barrier.

In vivo results showed a transient positive effect on tumor burden and volume around week 4 when treated with Methyldopa. Further studies need to be performed utilizing this drug to verify its capacity when applied as a preventive form of treatment. With this work MRI protocols have been optimized allowing easier detection of the tumors, in particular the smaller ones. In addition it is also possible to verify whether the tumors are leaky or not. This can then be used in future animal studies, to see whether leakiness changes as a function of treatment.

Index

Abbreviations X

List of Figures XIII

1) Introduction: 1
- **1.1) Principles of Cancer** 1
- **1.2) The Cell Cycle** 7
- **1.3) Melanoma** 8
- **1.4) Brain Metastasis** 9
- **1.5) Current Treatments** 9
- **1.6) Blood Brain Barrier and Drug Delivery** 10

2) Material and methods 12
- **2.1) Establishing Animal Models** 12
- **2.2) cMAP and drug selection** 12
- **2.3 Drugs** 13
- **2.4) Cell Culturing Techniques** 14
  - 2.4.1) Cell culturing 14
  - 2.4.2) Cell counting 15
  - 2.4.3) Freezing Cells 16
- **2.5) Cell Lines** 16
- **2.6) Monolayer viability assay** 18
- **2.7) DNA Cell Cycle Analysis** 19
- **2.8) Apoptosis Assay** 21
- **2.9) Soft Agar proliferation assay** 21
- **2.10) Principles of Animal Handling** 23
- **2.11) MRI** 25

3) Results 29
- **3.1) cMAP and Drug Selection** 29
- **3.2) *In Vitro* Studies** 31
  - 3.2.1) Monolayer Viability Assay 31
  - 3.2.2) Soft Agar proliferation 34
  - 3.2.3) Summary of all IC_{50} Results 36
  - 3.2.4 DNA Cell Cycle Analysis 37
  - 3.2.5) Apoptosis assay 40
- **3.3) *In Vivo* Studies** 45
  - 3.3.1) Experimental Layout 45
  - 3.3.2) In vivo Trichostatin A (TSA) treatment 45
  - 3.3.3) In vivo Pentamidine and Methyldopa treatment 46
  - 3.3.4) *In vivo* TSA 47
  - 3.3.5) *In vivo* Pentamidine/Methyldopa 50
  - 3.3.6) MRI Protocol Optimization 54

4) Discussion/Conclusion 55

5) Future aspects 58

6) References 59

Abbreviations

Abbreviation	Full name
ATP	Adenosine Triphosphate
Akt	Protein kinase B
BBB	Blood Brain Barrier
BLI	Bioluminescent Imagining
CAS	Chemical Abstracts Service
CNS	Central Nervous System
cMAP	Connectivity Map
CD36	Thrombospondin receptor
CTC	Circulating Tumor Cells
Da	Dalton
DNA	Deoxyribonucleic acid
DMSO	Dimethyl Sulfoxide
ECM	Extracellular Matrix
EMT	Epithelial – Mesenchymal Transition
ERK	Extracellular signal-regulated kinases
EtOH	Ethanol
FACS	Fluorescence-activated cell sorting
FDA	Food and Drug Administration
FGF	Fibroblast Growth Factor
FCS	Fetal Calf Serum
FS	Forward Scatter
GFP	Green Fluorescent Protein
GLUT1	Glucose Transporter 1
IC_{50}	The half maximal inhibitory concentration
IGF-1R	Insulin-like growth factor 1 receptor

IL-3	Interleukin 3
MET	Mesenchymal – Epithelial Transition
Melanoma	Malignant Melanoma of the Skin
MRI	Magnetic Resonance Imaging
MMP	Matrix Metalloproteinases
MT-MMP	Membrane Tethered matrix Metalloproteinases
MW	Molecular Weight
NSD	Norwegian Directorate of Health
nod/scid	Nonobese-diabetic/severe combined immunodeficient mouse
NS	Not Significant
PBS	Dulbeccos phosphate-buffered saline
PEN-STREP	Penicillin/Streptomycin
PI	Propidium Iodide
PMT	Photomultiplier Tube
pRB	Retinoblastoma Protein
RT	Room Temperature
RF	Radio Frequency
RPM	Rotations per Minute
REC	The Regional Ethical Committee
RCF	Relative Centrifugal Force
SD	Standard Deviation
SLC	Solute Carrier Family
SRS	Stereotactic Radiosurgery
SS	Side Scatter
T_1	Relaxation Time of Longitudinal Magnetisation
T_2	Relaxation Time of Transverse Magnetisation
T	Tesla

TSA	Trichostatin A
UV	Ultraviolet
UoB	University of Bergen
VEGF	Vascular Endothelial Growth Factor
WBRT	Whole-Brain Radiotherapy

List of Figures

Figure 1.1 Illustration of the hallmarks of cancer;

Figure 1.2 EMT in local invasion and intravasation;

Figure 1.3 The cell cycle;

Table 2.1 Table containing list of compounds;

Table 2.2 Components comprising cell culture medium and freezing solution;

Figure 2.1 Figure showing morphological aspect of cell lines used in this work;

Figure 2.2 Schematic representation of flow cytometry data analysis;

Figure 2.3 Image of a nod/scid mouse used in *In vivo* experiments;

Figure 2.4 Absorption of RF energy;

Figure 2.5 Representation of T1 and T2 curves;

Figure 3.1 Tissue sample generation, expression profiling, and Connectivity Map analysis;

Figure 3.2 Monolayer proliferation assay for Decamethonium Bromide, Fluticasone, Gabexate and Sulphapyridine in all cell lines;

Figure 3.3 Monolayer Viability assay for Lymecycline, Methyldopa, Lanatoside C, Trichostatin A and Pentamidine in all cell lines.

Figure 3.4 Soft agar proliferation assay for Lymecycline, Methyldopa, Lanatoside C, Trichostatin A and Pentamidine.

Table 3.1 Table containing IC_{50} values for all *In vitro* studies.

Figure 3.5 Cell cycle analysis of H1_DL2, H3, Melmet1 pGF1, and Melmet5 pGF1 by flow cytometry.

Table 3.2 Statistical information relative to cell cycle analysis, mean values ± SD of the whole experiment.

Figure 3.6 Apoptosis assay on H1_DL2 human melanoma metastasis cell line;

Figure 3.7 Apoptosis assay on H3 human melanoma metastasis cell line;

Figure 3.8 Apoptosis assay on Melmet1_pGF1 human melanoma metastasis cell line;

Figure 3.9 Apoptosis assay on Melmet5_pGF1 human melanoma metastasis cell line;

Table 3.3 Percentage of apoptotic cells for untreated cells, and cells treated with 100mM Pentamidine or 100mM Methyldopa:

Figure 3.10 Illustration of intercardiac injection and interperitoneal treatment

Figure 3.11 Representative MRI Scans of mice brains during TSA *In vivo* treatment over the period of the experiment;

Figure 3.12 Graph representing tumor burden and volume during treatment at week 8;

Figure 3.13 Graphic illustrating animal survival thought the course of the experiment;

Figure 3.14 Graphic illustrating animal weights thought the course of the experiment;

Figure 3.15 Representative MRI Scans of mice brains during Methyldopa/Pentamidine *In vivo* treatment over the period of the experiment;

Figure 3.16 Graph representing tumor burden and volume during treatment at week 4;

Figure 3.17 Graph representing tumor burden and volume during treatment at week 6;

Figure 3.18 Graphic illustrating animal survival through the course of the experiment;

Figure 3.19 Graphic illustrating animal weights throughout the course of the experiment;

Figure 3.20 Representative MRI Scans showing progress of MRI protocol optimization.

1) Introduction:

1.1) Principles of Cancer

In 2012, the worldwide burden of cancer rose to an estimated 14 million new cases per year, a figure expected to rise to 22 million annually within the next two decades. Over the same period, cancer deaths are predicted to rise from an estimated 8.2 million annually to 13 million per year. Globally, in 2012 the most common cancers diagnosed were those of the lung (1.8 million cases, 13.0% of the total), breast (1.7 million, 11.9%), and large bowel (1.4 million, 9.7%). The most common causes of cancer death were cancers of the lung (1.6 million, 19.4% of the total), liver (0.8 million, 9.1%), and stomach (0.7 million, 8.8%) (1).

Cancer cells are unlike most cells in the human body, which only divide when exposed to extracellular signals such as growth factors. Instead, cancer cells divide more or less continuously, ultimately forming tumors. By the time the tumor can be felt or found using current technologies, it already contains millions of cells. Tumors can be benign or malignant.

The most fearsome characteristic of cancer cells is their ability to invade surrounding tissues and spreading to other parts of the body using the circulatory and lymphatic system. When malignant cells become lodged in a distant part of the body, they divide and grow forming a new tumor at that new site. This process is called metastasis, (explained in more detail ahead); this often results in organ failures and makes cancer treatment very complicated (2).

Cancer has specific traits that are important to comprehend, as to fully understand the capacities of this disease and therefore be able to give a more generalized form of treatment. These traits are known as the “hallmarks of cancer” and are described below:

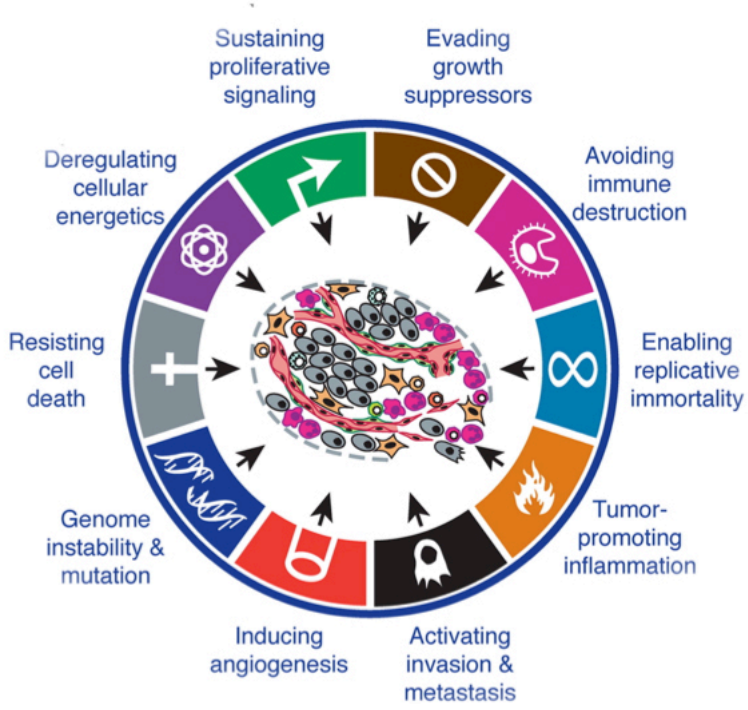

Figure. 1.1 – illustration of the hallmarks of cancer, adapted from (3).

- **Sustaining proliferative signaling**

Normal cells require external growth signals to proliferate, and these signals are transmitted through receptors that pass through the cell membrane. In contrast, cancer cells can grow and divide without external growth signals. Some cancer cells are autosufficent, generating their own growth factor molecules. Receptors themselves can be overexpressed. Or mutated ones can send signals without any growth factors at all (3).

- **Evading growth suppressors**

Cancer cells are generally resistant to growth-preventing signals from the neighbouring normal cells. The growth of normal cells is kept under control by growth inhibitors in the surrounding environment, in the extracellular matrix and on the surfaces of neighboring cells. These inhibitors act on the cell cycle clock, by interrupting cell division (mitosis) in the interphase.

Ultimately, the growth inhibitor signals are funneled through the downstream retinoblastoma protein (pRB), which prevents the inappropriate transition from (G_1) to S. If pRB is damaged through a mutation in its gene, or by interference from human papilloma virus, the cell can divide uncontrollably (3).

- **Avoiding immune destruction**

By disrupting the processes of the cancer immunity cycle throughout the body, tumors can avoid detection by the immune system and limit the extent of immune destruction. Some processes by which tumor cells avoid immune destruction is by disrupting antigen detection, inhibiting T-cell activation by dendritic cells, blocking T-cell infiltration into tumor and suppressing cytotoxic T-cell activity (3, 4, 5).

- **Enabling replicative immortality**

Non-cancer cells die after a certain number of divisions or go into quiescence. Some types of cells, such as nerve and heart muscle cells, become quiescent when they reach maturity but continue to perform their main functions for the rest of the organism's life. Multinucleated muscle cells that do not undergo cytokinesis are also often considered to be in the G_0 stage. Cancer cells escape this limit and are apparently capable of indefinite growth and division, becoming immortal. But those immortal cells have damaged chromosomes, and can become cancerous.

Mammalian cells have an intrinsic program, the Hayflick limit, that limits their multiplication to about 60–70 doublings, at which point they reach a stage of senescence. This limit can be overcome by disabling their pRB and p53 tumor suppressor proteins, which allows them to continue.

The counting device for cell doublings is the telomere, which loses DNA at the tips of every chromosome during each cell cycle. Many cancers involve the upregulation of telomerase, the enzyme that maintains telomeres length (3).

- **Activating invasion & metastasis**

Initiation of metastasis requires invasion, which is enabled by EMT (Epithelial – Mesenchymal Transition) (**Figure. 1.2)**. Carcinoma cells in primary tumors lose cell-cell adhesion mediated by E-cadherin repression and break through the basement membrane with increased invasive properties, and enter the bloodstream through intravasation. Later, when these circulating tumor cells (CTCs) exit the bloodstream to form micrometastases, they undergo MET (Mesenchymal – Epithelial Transition) for clonal outgrowth at these metastatic sites. Thus, EMT and MET form the initiation and completion of the invasion-metastasis cascade.

A partial loss of E-cadherin, the caretaker of the epithelial state, is associated with carcinoma progression (6). During EMT, E-cadherin gene transcriptional repression, promoter methylation, and protein phosphorylation and degradation have all been observed (7, 8)**.** In order to invade through local basement membrane (surrounding the tumor or the tumors vasculature), these mesenchymal tumor cells up-regulate several secreted (MMPs) and membrane-tethered (MT-MMPs) proteases to break down ECM components (3).

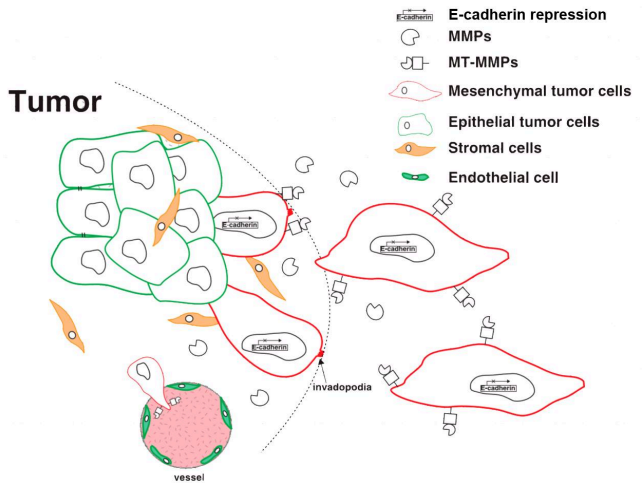

Figure. 1.2 - EMT in local invasion and intravasation. Activation of the EMT program is mostly characterized by loss of E-cadherin expression. In order to invade through local basement membrane, these mesenchymal tumor cells up-regulate several secreted (MMPs) and membrane-tethered (MT-MMPs) proteases to break down ECM components. Adapted from (9)

- **Tumor promoting inflammation**

The tumor microenvironment is often infiltrated by innate and adaptive immune system cells, which enable tumors to mimic inflammatory conditions seen in normal tissues. This will promote tumor progression by supplying the tumor microenvironment with growth factors, survival factors, pro-angiogenic factors, extracellular matrix (ECM) – modifying enzymes that promote angiogenesis, invasion, and metastasis and also inductive signals that activate epithelial-mesenchymal transition (EMT) (3).

- **Inducing angiogenesis**

Angiogenesis is the process by which new blood vessels are formed. Cancer cells appear to be able to kickstart this process, ensuring that such cells receive a continual supply of oxygen and other nutrients.

Cancer cells initially lack angiogenic ability, limiting their ability to expand. In order to progress, they must develop a blood supply. Inducers and inhibitors balance angiogenesis. Inducers include vascular endothelial growth factor (VEGF) and acidic and basic fibroblast growth factor (FGF 1/2), which bind to transmembrane tyrosine kinase receptors displayed on endothelial cells. An inhibitor is thrombospondin-1, which binds to CD36. Thrombospondin-1 is regulated by p53, so loss of p53 can promote angiogenesis.

Angiogenesis is involved in the growth of all tumors, but most pronounced in cervix, breast and melanoma tumors (3).

- **Genome instability & mutation**

Multiple alterations in the genomes of cancer cells serve as the foundation for many oncogenic processes. Cancer cells take advantage of increased rates of mutations in order to accumulate several mutations needed to foster carcinogenesis. They do this through increased sensitivity to mutagenic agents and/or a breakdown in one or more of the cell's DNA repair mechanisms mediated by genes such as *p53* or breast cancer type 1 susceptibility protein (*BRCA1*). Also when caretaker genes are inactivated or suppressed, tumor cells can increase the rate of mutations and, subsequently, tumorigenesis (3, 10).

- **Resisting cell death**

Apoptosis is a form of programmed cell death (cell suicide), the mechanism by which cells are programmed to die in the event they become damaged.
Apoptosis can be triggered by an overexpressed oncogene, and this may be the primary means by which such mutant cells are continually removed. Conversely, cancer cells must overcome apoptosis to progress.

The apoptotic machinery can be divided into sensors, which monitor the cell for abnormal behavior, and effectors, which cause apoptosis. The sensors include survival signals and their receptors, which monitor the cell for DNA damage, oncogene overexpression, and low oxygen (hypoxia). They monitor survival signals from the cell matrix and neighboring cells.
Sensors include IGF-1/IGF2 and their receptor IGF-1R; and IL-3 and its receptor. The effectors include FAS ligand and its receptor, and TNF-α and its receptor. The p53 tumor suppressor protein elicits apoptosis in response to DNA damage, and is a major mechanism of cancer control. In order for cancer to progress, it must overcome p53, and in fact, p53 is mutated in half of all cancers (3)**.**

- **Deregulation of cellular energetics**

To sustain uncontrolled proliferation, cancer cells make adjustments to their energy production by reprogramming their glucose metabolism, upregulating glucose transporters such as glucose transporter 1 (GLUT1) and depending on alternate metabolic pathways.

Although limiting energy production to the glycolysis phase decreases the amount of adenosine triphosphate (ATP) produced, it also allows cancer cells to divert glycolic intermediates to various pathways, including those required to assemble new cells (3).

1.2) The Cell Cycle

The cell cycle is controlled by specific checkpoints, which stop the cells from progressing to next phase or completing the current one. These checkpoints ensure completeness of the genome and that the stage of the cell cycle is properly completed before the next phase is begun. The S phase, which concerns DNA replication, is followed by the M phase or mitosis, which involves chromosome segregation, and the cycle is continued by cell division. There are three internal checkpoints that evaluate the eukaryotic cell cycle:

- G1/S: cells check whether they should continue through division or enter a resting stage and whether their genome is able to divide.
- G2/M boundary: cells check whether their DNA is fully replicated and undamaged before progression into the M phase. If not, the cell cycle is arrested in the S-G2 by inactivation of Cdc25 and activation of Wee1.
- Metaphase/anaphase: cells check whether all chromosomes are attached to the bipolar mitotic spindle via their kinetochores and whether the sister chromatids are ready for separating from each other (11).

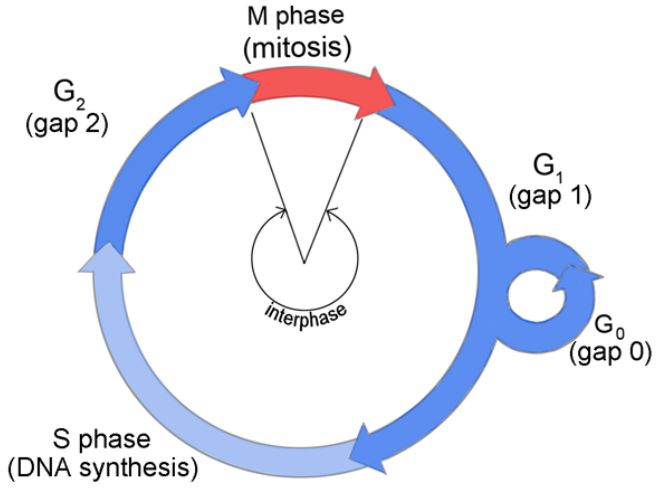

Figure.1.3 – The cell cycle. The cell grows continuously in interphase, which consists of three phases: DNA replication is confined to S phase; G1 is the gap between M phase and S phase, while G2 is the gap between S phase and M phase. In M phase, the nucleus and then the cytoplasm divide. Some cells become quiescent when they reach maturity and do not undergo cytokinesis are also often considered to be in the G_0 stage, image from (12).

Checkpoints are meant to stop the cell cycle when genome integrity is damaged. Hence cells with genetic mutations are prevented from further division, and transition of the fault into subsequent cell generations is prevented. Cells with damaged DNA become arrested in these checkpoints. Arrest in G1 prevents copying of damaged bases and arrest in G2 allows cells to repair DNA double-strand breaks.

The cell cycle and its checkpoints are working properly and perfectly in a healthy body. However sometimes some random stimuli like genetic mutations or UV light disturb the natural balance and can induce repression of tumor suppressor genes or overexpression of oncogenes, thus leading to tumor development (13).

1.3) Melanoma

Malignant melanoma is the ninth most common cancer in Europe and the 19th most common cancer worldwide, with around 232,000 new cases diagnosed in 2012 (14, 15).

The main known risk factor for melanoma is sunlight exposure. Other risk factors that can increase the incidence of melanoma are ultraviolet radiation, skin and hair type as well as eye color, family history (hereditary mutation), previous cancer (metastasis) and radiotherapy, as well as a weakened immune system (16).

Melanomas most often arise within epidermal melanocytes of the skin, although they can also originate from melanocytes such as those lining the choroidal layer of the eye, gastro intestine & genitourinary system mucosal surfaces, or the meninges. Melanoma is also among the most common cancer to metastasize due to its invasive properties. Clinical staging for primary cutaneous melanoma employs measurements of thickness (in millimeters), presence of ulceration, penetration through cutaneous layers, mitotic rate, evidence of “in transit” metastasis, tumor spread to draining lymph nodes, and evidence of distant metastasis. Management issues in melanoma can be classified in terms of prevention, diagnosis, local disease management, and treatment of metastatic disease (17).

1.4) Brain Metastasis

Brain metastasis is the leading neoplastic disease in the human central nervous system (CNS) **(**18). It usually ascertains itself at the end stage of the disease's advancement and causes a sharp deterioration in patients' life quality (19). The period of latency differs depending on the tumors origin. Formation of brain metastasis is a common outcome for 40% to 60% of melanoma patients (20, 21, 22)

In general, brain metastatic tumors are resistant to chemotherapy and even some newly emerged targeted therapeutic regimens. The blood-brain barrier (BBB) is known as the major obstacle for delivering drugs to the site of tumor cells inside the brain, due to low drug penetration **(18).** Therapeutic approaches are being selected based on the type of primary cancer, the number and location of the metastatic lesions as well as the stage of cancer. Current standard treatment for patients with brain metastasis is surgical resection followed by radiotherapy, and sometimes chemotherapy. These treatments may decrease the chance of recurrences of brain metastasis, and can increase the patient's quality of life (23). Precise considerations must be applied before choosing a proper treatment. A convenient selection of pharmacological agents can help patients with certain hindering symptoms. However, an unjustified choice of treatment could lead to a reduction in the patient's quality of life. In general, the life expectancy for patients with brain metastasis is poor, around 6 months regardless of treatment (22).

1.5) Current Treatments

Nowadays treatment for brain metastasis relies mainly on surgery, radiotherapy, chemotherapeutic agents or a combination of these. Due to the poor prognosis and lack of uniform approaches to therapy and assessments, patients with brain metastases have also been routinely excluded from clinical trials of new agents and were also thought unlikely to benefit from immunotherapy, in part because of the immunosuppressive effects of glucocorticosteroids. Standard radiotherapy approaches include stereotactic radiosurgery (SRS) or whole-brain radiotherapy (WBRT) (24). SRS, a precise focusing of radiation (Cyberknife and Gamma Knife) on well-defined individual intracranial lesions, is used just on a few well circumscribed metastatic lesions from melanoma brain metastases, barring issues

that warrant urgent surgery such as hemorrhage or mass effect and remains the standard of care (25) SRS without WBRT may also be a viable option in patients with one or few metastases and contraindications for surgery. WBRT, in contrast, involves irradiation of the entire brain with a uniform dose. SRS and WBRT are both used as primary or adjuvant therapies in patients with melanoma and brain metastases; notably, however, comparisons of surgical resection followed by WBRT and WBRT alone in these patients have not yielded definitive results (26).

Chemotherapy alone is generally ineffective for the treatment of melanoma CNS metastases. Failure of systemic treatment for brain metastases in the past has been blamed on the inability of most experimental agents to pass the blood–brain barrier in addition to the low activity of these agents against melanoma (18, 27).

Until recently, no compounds have demonstrated a significant survival benefit for patients with melanoma who develop brain metastases, and the prognosis for these patients has remained poor.

1.6) Blood Brain Barrier and Drug Delivery

Circulating tumor cells that reach the brain must pass through the BBB in order to form metastatic colonies in the brains parenchyma. Previous studies have demonstrated that endothelial cells lining the blood vessels in the brain are distinct from the endothelial cells in other organs (28). There are tight junctions between the endothelial cells that cover the internal walls of the vessels, forming a continuous sheath, which inhibits free, transcapillary movement of polar molecules. In addition, astrocytic endfeet and pericytes make up a continuous outer layer, further restricting access to the brain. Additionally, efflux transport proteins localized on the endothelium further diminish the effectiveness of circulating drugs by pumping them back to the blood circulation (29). Besides being a primary barrier for cancer cells, endothelial cells also play an important role in supporting the development of brain metastasis (30).

The unique anatomy of the BBB provides a cellular barrier between the circulating blood and the interstitial fluid (31). It is also important for the homeostatic regulation of the brain and CNS functions (32). Tome Teese, Morris Karnovsky, and Milton Brightman

demonstrated the role of the BBB for the first time in the 1960s. By using electron microscopy, they showed is the presence of a barrier that prevents passage of injected electron-dense agents such as lanthanum salts. The BBB also works as a detoxification layer in the brain by assisting in removal of xenobiotics compounds from the brain.

Any substances that are trying to reach the brain need to pass through the endothelial cell membranes. However, hydrophilic molecules such as glucose and amino acids, which supply the extensive metabolic needs of the brain, may overcome the lipophilic constrain. The fact that glucose easily pass through the BBB can be considered as proof for the presence of more complicated regulatory systems (33). The main pathway for hydrophobic substances to reach the brain is transcellular diffusion with the help of specialized proteins like solute carrier family (SLC), which has been shown to be effective in the flow of organic compounds, especially organic anions, through the BBB (34, 35). Other methods of transportation through BBB are achieved by energy dependent, active transporters, for instance the adenosine triphosphate (ATP)-binding cassette (ABC) family, which is mostly present at the luminal side of the BBB (36).

In general, substances with a molecular weight above 500 Da are usually not able to penetrate the BBB. However, the complexity of the BBB means that charge, lipophilicity, binding to plasma proteins, and size of a molecule all must be taken into account when determining permeability of a drug through the BBB (37). Previous studies have shown that there was no efficient penetration of several hydrophobic molecules within the preferable range of molecular weight (38).

2) Material and methods

2.1) Establishing Animal Models

Many existing animal models for modelling cancer metastasis are murine derived, and thus likely do not reflect the same genetic and epigenetic changes as found in human cancers. Several models have also been derived, using orthotopic xenografts. However, these models show a rare incidence of brain metastasis, making them sub-optimal in brain metastatic research. Therefore, Prof. Thorsens research group has developed novel model systems, where human brain metastasis tumor cell lines from melanoma, lung adenocarcinomas or human breast cancers are injected systemically into nod/scid mice. The cell lines were injected into the left cardiac ventricle in mice, and tumor development was studied by bioluminescent imaging (BLI). During 3-6 weeks, all animals developed new tumors with a clear preference to the brain. T1 and T2 weighted (T1w and T2w) MRI showed multiple metastases within the brain, similar to what is seen in patients, and histology confirmed these findings. The models are thus among the very few which, in a systematic and consistent manner, can mimic the metastatic spread of cancers seen in patients. These models recapitulate most of the steps of the metastatic cascade, and thus provide a better tool to obtain information on the molecular mechanisms behind brain tumor metastasis.

2.2) cMAP and drug selection

After intracardiac injections, tumor burden was seen mainly in the animal brains, and to some extent in bone, adrenals and ovaries. These organs were removed after sacrificing the animals, the organs were dissociated, and tumor cells were sorted out by FACS. Transcriptome profiling with RNA-sequencing was performed on triplicate tumor samples from each organ, on a Illumina HiSeq 2000 platform (at BGI@UC Davis, Sacramento, CA).

2.3 Drugs

The task in my Master work was to screen 9 out of the 10 remaining drugs for *in vitro* and *in vivo* treatment efficacy. These drugs are listed in the table below.

Table. 2.1 - Table containing list of compounds. Also present here are all details relative to molecular weigh, dose usually administered, cMAP score and main applications of these drugs.

Compound	MW [Da]	Dose [µM]	cMAP Score	Medical conditions where the drug is used
Decamethonium Bromide	418,29	10	-0,871	Interrupts transmission at the skeletal neuromuscular junction by causing sustained depolarization of the motor end plate, skeletal muscle relaxation.
Sulfapyridine	249,29	16	-0,872	A sulfanomide antibacterial.
Pentamidine	340,42	7	-0,873	Antimicrobial medication for prevention and treatment of pneumocystis pneumonia. Also used as prophylactic against PCP in patients receiving chemotherapy.
Lymecycline	602,63	7	-0,878	A tetracycline broad-spectrum antibiotic.
Fluticasone	444,51	8	-0,88	Fluticasone propionate is a corticosteroid derived from fluticasone used to treat asthma and allergic rhinitis. It is also used to treat eosinophilic esophagitis.
Lanatoside C	985,12	4	-0,882	A cardiac glycoside, a type of drug that can be used in the treatment of congestive heart failure and cardiac arrhythmia (irregular heartbeat).
Trichostatin A	302,37	1	-0,887	An antifungal antibiotic and selectively inhibits the class I and II mammalian histone deacetylase. TSA has some potential as an anti-cancer drug.
Methyldopa	275,73	15	-0,904	Reduces high blood pressure (antihypertensive).
Gabexate	311,37	19	-0,912	A serine protease inhibitor used (as Gabexate Mesylate) in the treatment of pancreatitis, intravascular coagulation, and as a anticoagulant for haemodialysis.

2.4) Cell Culturing Techniques

2.4.1) Cell culturing

The cell culture work was performed under sterile conditions inside a laminar airflow hood. All the working surfaces and equipment were disinfected with 70% ethanol prior to working and when finished. The cells were kept in incubation flasks and multi-well dishes, which were put in the incubator at 37ºC, 5% CO_2 and 100% relative humidity. Solutions and disposables frequently used for cell culture are listed below.

Table. 2.2 - Components comprising cell culture medium and freezing solution.

Chemical		**Supplier**
ALT DMEM		
Dulbeccos Modified Eagles Medium	450mL	Sigma-Aldrich Inc. MO, USA
Heat inactivated fetal calf serum (FSC)	50mL	Fischer Scientific, MA, USA
L-Glutamine, 200nM	10mL	BioWhittaker, Verviers, Belgium
Penicillin/Streptomycin (PEN-STREP), 100uL/mL	10mL	BioWhittaker, Verviers, Belgium
Non essential amino acids 100x	16mL	BioWhittaker, Verviers, Belgium
Plasmocin, 25mg/mL	0.1mL	Invivogen, CA, USA
Dulbeccos phosphate-buffered saline (PBS)		Sigma-Aldrich Inc.
Trypsin EDTA, 0.25%		BioWhittaker
Freezing solution1:		
ALT DMEM	9mL	
FCS (Fetal calf serum)	1mL	
Freezing solution 2:		
1×PBS	8mL	
Dimethyl sulphoxide (DMSO)	2mL	
Disposable pipettes: 5, 10, and 25mL		Sigma-Aldrich Inc

The cells were grown in growth medium supplemented with 10% heat-inactivated newborn calf serum, four times the prescribed concentration of non-essential amino acids, 2% L-glutamine, penicillin (100 IU/ml), and streptomycin (100 µl/ml) (hereafter called ALT DMEM). The growth medium was exchanged twice a week. The cells were kept in medium sized blue filtered cap culture flasks (Nunc AS, Roskilde, Denmark) between experiments. The cells were regularly passaged when they reached 70-80% confluency. The old growth medium was removed, and the cells were washed with 3mL PBS. The PBS was then removed, and 3mL trypsin was added into the flask. After 3-4 minutes (when the cells were detached from the plastic surface) 4mL ALT DMEM was added in order to neutralize the effects of the trypsin. One third of the cell solution was then transferred to a new growth flask, and 25mL ALT DMEM was added.

2.4.2) Cell counting

It was important to add the correct amount of tumor cells into each well of the dishes, when performing the proliferation assays. Thus, each experiment started by counting the number of cells in the culture flasks. The large sized flasks containing the cells were trypsinized with 4mL trypsin, followed by adding 5mL ALT DMEM into the culture flask. The cell solution was then transferred into sterile conical centrifuge 15mL tubes (Nunc, Thermo Scientific, NY, USA). We then determined the cell concentration using a Countess ® Automated cell counter (Life Technologies, NY, US) based on the manufactures instructions: 10µl of cell solution were mixed with 10µl of Trypan blue (Life Technologies, NY, US) to exclude dead cells and thereafter pipetted into the Countess ® chamber slides. The chamber slide was placed into the cell counter, and the focus was adjusted to obtain a clear image of the cells. By pushing the "START" button on the machine the number of cells within the slide was automatically calculated and the cell counter showed the number of live cells, dead cells as well as the total number of cells, on the display. Each cell counting experiment was performed in duplicate.

2.4.3) Freezing Cells

All cell lines were used only for 12-15 passages before discarded, in order to minimize any potential, phenotypic drift of the cells. Thus, several samples of each cell line were frozen in liquid nitrogen, to ensure that we always had access to new and viable batches.

The cells were first checked using the in-lab light microscope (TMS, Nikon Instruments Inc., NY, USA), to verify whether healthy and adequate in number. The cells were trypsinized, ALT DMEM was added, and the cell solution was transferred into 15mL tubes. The cells were then centrifuged at 900rpm for 4 minutes, and the growth medium was removed from the cell pellet. The freezing solution was then gently added into the tube, the cells were re-suspended, and 1mL of cell solution was transferred into each of 1.5mL cryotubes (Thermo Scientific Inc., MA, USA). The freezing solution was a mix of 2 different solutions, as described in Table 2.2. The vials were wrapped in tissue and placed in a freezer at -80º C over one night, in order to let them cool down slowly. Then they were transformed to the nitrogen liquid tank for long-term storage.

2.5) Cell Lines

Four melanoma metastasis low passage culture cell lines (Melmet1 pGF1, Melmet5 pGF1, H1_DL2 and H3) were used in these experiments. Written consents were obtained from the patients before tumor material was collected. The Regional Ethical Committee (REC Number 013.09) and the Norwegian Directorate of Health (NSD Number 9634) approved the tissue collection and biobank storage of tumor biopsies and derived cell lines.

The H1 and H3 cell lines were previously established in Prof. Thorsens lab, from melanoma brain metastasis of admitted patients at the Haukeland University Hospital, Bergen, Norway. The H1 cells were transduced with two lentiviral vectors, encoding Dendra (a green fluorescent protein (GFP) variant) and luciferase to obtain the H1_DL2 cell line.

The Melmet1 and Melmet5 cell lines were a generous gift from Professor Øystein Fodstad (Dept. of Tumor Biology, the Norwegian Radium Hospital, Oslo, Norway)(5). Melmet1 was established from subcutaneous metastases of a 36-year-old female melanoma patient. This particular cell line have demonstrated invasive potential but low intrinsic proliferation in comparison to Melmet5 which shows a larger proliferation capacity. Melmet5

was established from a lymph node metastases of a 56 year old male melanoma patient. They have low invasive capacity and as mentioned before a rapid proliferation ability. These cells have a strong tendency to metastasize to the brain, lung, liver and bone (in vivo). The Melmet 1 and Melmet 5 cells were transduced with a lentiviral vector, encoding CopGFP (a GFP variant) and Luciferase, resulting in the Melmet 1 pGF1 and Melmet 5 pGF1 cell lines.

All cells were grown in ALT DMEM. The cells were kept in a standard tissue culture incubator at 37 °C with 100% humidity and 5 % CO_2. The growth medium was exchanged twice a week.

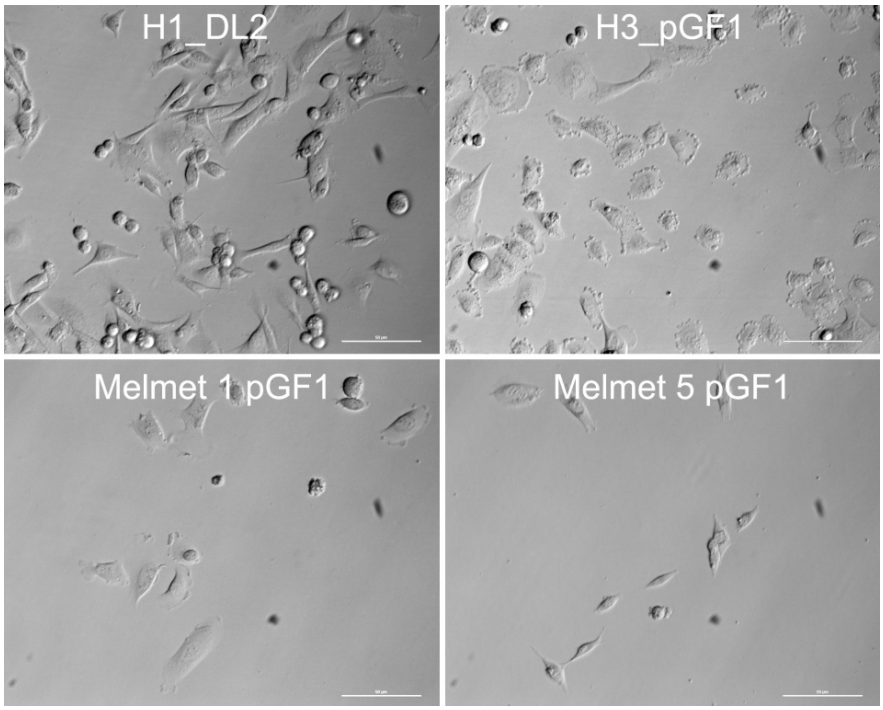

Figure. 2.1 – Figure showing morphological aspect of cell lines used in this work, scale bar 50µm.

2.6) Monolayer viability assay

The monolayer viability assay is based on the enzymatic reduction of resazurin by viable cells. Resazurin comes as a sodium salt (Sigma Aldrich, ST. Louis, MO, US), and was diluted to a stock solution of 1mg/mL in PBS (Sigma Aldrich). The stock solution was frozen at -20ºC until use. Before use, the stock solution was thawed and mixed with PBS to a working concentration of 0.1mg/mL. The amount of applied resazurin was 10% of the current volume of solution in the well or the dish.

Three 96-well plates (Nunc, Thermo Scientific, USA) for each cell line were prepared with 8×10^3 cells/100µL into each well of the plate. After 24 hours of incubation to make sure the cells were attached to the surface, 100 µL of drug was added into each well, to obtain the following concentrations, 0.001 µM, 0.01 µM, 0.1 µM, 0.5 µM, 1 µM, 2.5 µM, 5 µM, 50 µM, 100 µM or 500 µM. One column in each 96-well plates contained only cells and medium, without drug (negative control). Another column contained only medium, without adding cells or drug, and was used for calculation of background signal from the medium. As most of the drugs were dissolved in DMSO, a control of DMSO (0.01µM in ALT DMEM) was also prepared to ensure that this had no effect with cell viability, which was proved. After 72 hours of drug exposure, 20µL resazurin was added into all wells in the 96-well dish. Following incubation for 4 hours, the absorbance was measured at dual mode, at wavelengths of 560/590 nm absorbance value with a scanning multiwell spectrophotometer (Victor 3 1420 multi-label counter, Perkin Elmer, Waltham, MA, USA) using WorkOut v2.0 software (Dazdag Solution Ltd. East Sussex, UK), which created an Excel spreadsheet with the measurement data, as the output of the experiment.

All the results were transformed and prepared using the GraphPad Prism v6 software (GraphPad software, Inc, La Jolla, CA, USA). The data was normalized in Excel before being transferred to GraphPad Prism, where the data was transformed into a logarithmic form before fitted into a curve using a normalized response – variable slope logistic nonlinear regression analysis.

This experiment was performed on all nine compounds.

2.7) DNA Cell Cycle Analysis

Treatment of cells started by seeding 1.5×10^5 cells into each well of a 6-well plate (Nunc, Thermo Scientific, USA). After 24 hours of incubation and making sure that the cells had attached to the surface, 100μM of either Methyldopa or Pentamidine was added to three of the wells. The other three wells were controls and only received ALT DMEM. Exposure to drug continued for 48 hrs before the samples were prepared for flow cytometric analysis. The experiments were performed for all four cell lines.

The important point was to collect the cells and prepare the fixed samples while they were at approximately 70% confluency. It is important to avoid 100% confluency, as this will change the cell cycle towards more cells in the G1 phase.

The fixation step began by removing the medium in each well, and adding 0.5mL trypsin. When the cells had detached from the surface, 1.0mL ALT DMEM was then added, the cell solution was transferred into sterile 15mL tubes, and centrifuged at 500rpm for 5 minutes. The growth medium was then gently removed from the cell pellet, 100% ice cold EtOH was added, and the cells were re-suspended to obtain a homogeneous solution of cells. The cells were kept in the fridge (at 4ºC) until analysis.

As final preparation before flow cytometry analysis, the fixed samples were collected from the fridge and centrifuged at 900rcf for 5 minutes, the EtOH was removed and then 50μL 1mg/ml RNase (diluted in 1×PBS) and 150μL PI (Propidium Iodide) (50μg/ml) was added to the tubes. PI is fluorescent molecule that is used to stain the cells nuclei and has an excitation wavelength of 488 nm (39) and emits at a maximum wavelength of 617 nm. The samples were incubated at room temperature (RT) for 30 minutes in the dark to provide enough time for the RNase to dissolve free RNA in the cell solution (which otherwise would have been stained by PI, giving a false readout). The cell solution was transferred into a 2mL Eppendorf tube (Eppendorf AG, Hamburg, Germany) after passing through a cell strainer (Becton Dickinson Biosciences, MA, USA) and was mixed by a vortex mixer to make sure that the pellet was dissolved. All samples were analyzed using a BD AccuriC6 flow cytometer (Becton Dickinson Biosciences, NJ, USA). The fluorescence intensities were quantified by gating a two-parameter FL2-A and FL2-H cytogram to a one-parameter red fluorescence intensity plot. The data was further analyzed using Flowjo software (FlowJo, LLC, Ashland, OR, USA), to determine the % of cells in the different phases of the cell cycle. In this experiment, a peak area of FL2-H was recorded at 561 nm on a linear scale for the determination of cell cycle analysis, (39).

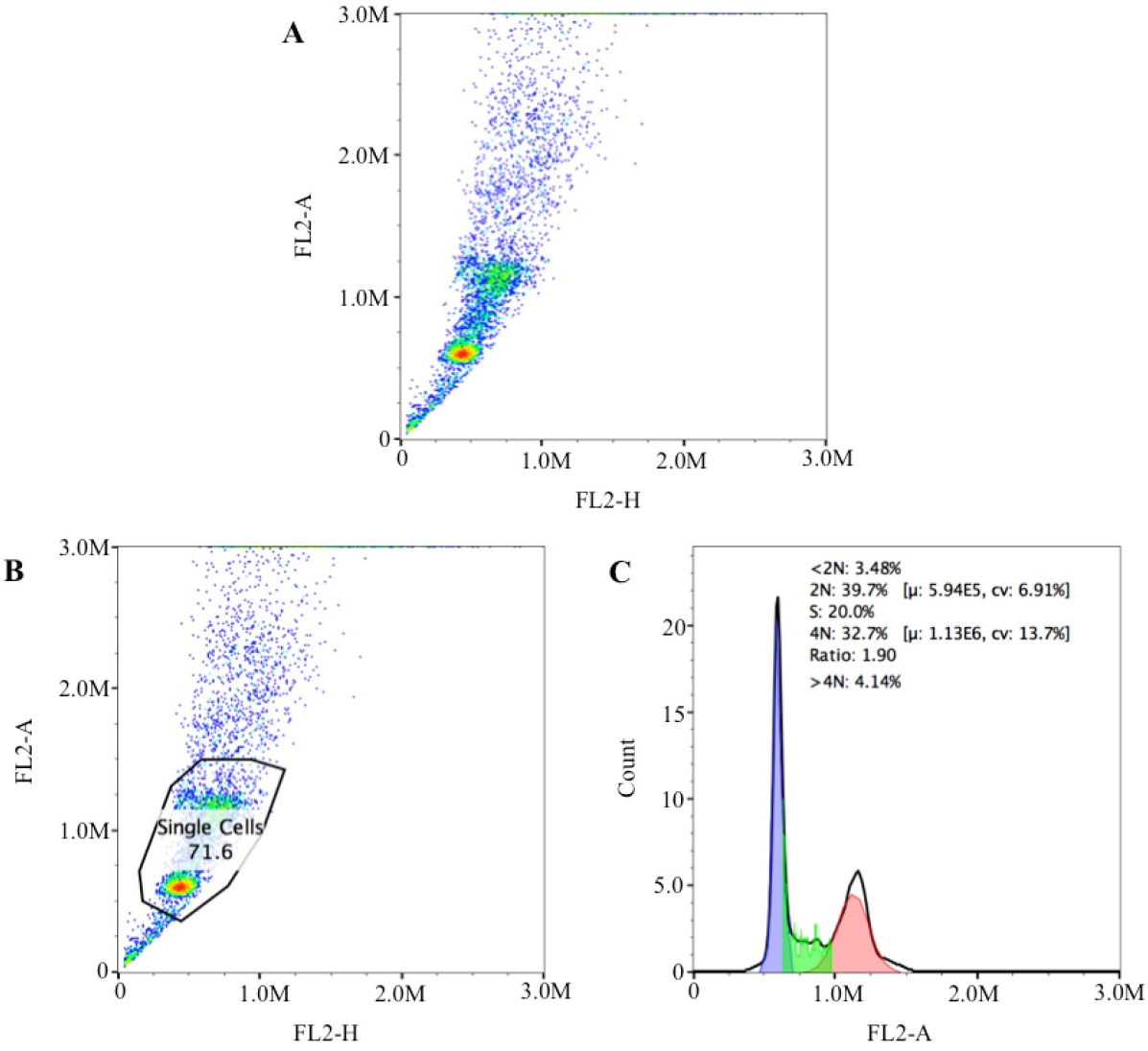

Figure. 2.2 – Schematic representation of flow cytometry data analysis: A representing raw flow cytometry data, **B** represents single cells within the circle, also called gate (the registered point outside the gate is either doublets or debris) and **C** cell cycle analysis (of the cells shown within the gate in Fig B).

The data was analyzed using FlowJo software (FlowJo, LLC, Ashland, OR, USA). In FlowJo, after sorting the selected cell population into by adjusting the scale of the axis, viable cells were gated from the debris and other residue, see figure 2.4 –B and C. By using the provided software through univariate analysis of fractions of cells, cell cycle for the determined population was derived using DNA binding dye PI. The histogram shows G1, S and G_2/M phases of the cell cycle under the categories of 2N, S, and 4N. It also revealed duration of each phase, and possible shift, figure 2.4 – C (40).

2.8) Apoptosis Assay

First, 5×10^4 cells were seeded into each well of a 24-well plate (Nunc, Thermo Scientific, USA). After 12 hours of incubation, Methyldopa or Pentamidine were added into the wells at a concentration of 100mM. The cells were exposed to the drug for 72 hours. Cells exposed to 10mM H_2O_2 for 4 hours were used as positive controls. Thereafter, 80µL Rose Bengal (concentration 1mg/mL; Sigma Aldrich, MO, USA) was added into each well, and incubated for 30 minutes at 37°C.

Cells were then collected and prepared for flow cytometric analysis. The top part of the medium in the wells was carefully collected using a 1mL pipette, and discarded. The remaining 1mL of medium, containing floating apoptotic cells, was collected in a 2mL eppendorf tube. 500 mL of PBS where then immediately added into the well to wash the plate, and the PBS was then transferred into the same eppendorf tube. In the next step, 500mL trypsin was added into the well and left in the CO_2 incubator for a few minutes to detach the cells, and then transferred to the previous fractions. This procedure was repeated for all wells in the 24-well plate. All tubes were centrifuged (1×1000 rcf eppendorf centrifuge, 3 minutes at 4°C). The supernatant was carefully removed, and the cells were washed twice, by re-suspending the cell pellet in 900mL PBS, followed by centrifugation as described above. Finally, the supernatant was removed, and the cell pellet was re-suspended in 100mL PBS. The samples were then analyzed on AccuriC6 flow cytometer, in a two parameter FL2-H by FL2-A cytogram, and thereafter analyzed further using the FlowJo software, as previously described in Chapter 2.7.

2.9) Soft Agar proliferation assay

Agar is a gelatinous substance, which is difficult to work with, as it hardens quickly in room temperature. In this assay, it was necessary to mix the tumor cells with liquid agar, thus it was essential to keep the agar at 37 ºC during this procedure. This assay includes three different steps: first preparing base agar, then preparing soft agarose overlay, and finally adding the drug solution.

1) Preparing base agar: For base agar preparation, 2.4% Difco Agar Noble (Becton Dickinson Biosciences, NJ, USA) was prepared by dissolving 0.48g Agar Noble in 20mL

autoclaved water (milliQ) in a glass bottle, warmed in a microwave and stirred until completely dissolved and homogeneous. Agar Noble solution and 60mL ALT DMEM were then warmed to 50^0C in a preheated water bath, and 3 parts of medium was mixed with 1 part of Agar Noble solution (3:1). 50μL of this mix was administered into each well in a 96-well plate and left at room temperature, to cool down.

2) Soft agarose overlay: A low melting point agarose (Sigma-Aldrich) was then prepared and overlaid on top of the base agar solution. 0.48g of low melting point agarose was mixed with 20mL milliQ water in a glass bottle (2.4% solution), and microwaved until dissolved. The solution was then kept in preheated water bath together with ALT DMEM for approximately 10 minutes. The agarose solution was mixed with ALT DMEM (1 part agarose solution and 3 parts of ALT DMEM) and placed back into the water bath. At this point the temperature of the water bath was decreased to 40^0C. Meanwhile, the cell solutions were prepared at a concentration of 1.6×10^5 cells/mL in ALT DMEM and were kept in the 15mL tubes in the CO_2 incubator. Two packages of filtered disposable pipette tips were placed in the CO_2 incubator as well. One at a time, the tubes containing cell suspension were mixed with agarose overlay/ALT DMEM solution (1:1 mix). 50 μL of this mixture was administered, with preheated filtered pipette tips, on top of base agar in each well of the 96-well plates. Afterwards, the plates were placed in a refrigerator for 30-35 minutes in order to prevent the cells from subsiding to the bottom of the soft agarose layer.

3) Adding the drug solution. After 30 minutes the plates were fetched from the fridge and the wells were overlaid with ALT DMEM containing drugs, to final desired concentrations (0.001 μM, 0.01 μM, 0.1 μM, 0.5 μM, 1 μM, 2.5 μM, 5 μM, 50 μM, 100 μM or 500 μM).

Afterwards, the plates were left in the incubator for several days for the cells to form spheroids. The incubation time was different for the different cell lines. Melmet5 pGF1 had formed a lot of detectable spheroids after 7 days, while it took H1_DL2 and Melmet1 pGF1 10 days to form spheroids. For the H3 cell line, it took 14 days to reach adequate numbers of spheroids. Resazurin was added to each plate and after 4 hours of incubation, each plate was analyzed in the spectrophotometer, followed by analysis in GraphPad Prism v6 as described in Section 2.5. This assay was repeated 3 times for each cell line and each drug.

2.10) Principles of Animal Handling

First and most importantly of all who care for, use, or produce animals for research, testing, or teaching must assume responsibility for their well-being. The principles of animal laboratory science used to uphold the scientific rigor and integrity of biomedical research with laboratory animals are expected to be followed by all.

Both researchers and institutions have affirmative duties of humane care and use that are supported by practical, ethical, and scientific principles. This system of self-regulation establishes a rigorous program of animal care and use and provides flexibility in fulfilling the responsibility to provide humane care. The specific scope and nature of this responsibility can vary based on the scientific discipline, nature of the animal use, and species involved, but because it affects animal care and use in every situation this responsibility requires that all that work with animals carry out purposeful analyses of proposed uses of laboratory animals.

Following the European animal welfare (EWA) rights all animals must be treated humanely;

- Freedom from hunger and thirst;
- Freedom from discomfort;
- Freedom from pain, injury and disease;
- Freedom to express normal behavior;
- Freedom from fear and distress. (EWA)

Humane care means those actions taken to ensure that laboratory animals are treated according to high ethical and scientific standards. Implementation of a humane care program, and creation of a laboratory environment in which humane care and respect for animals are valued and encouraged.

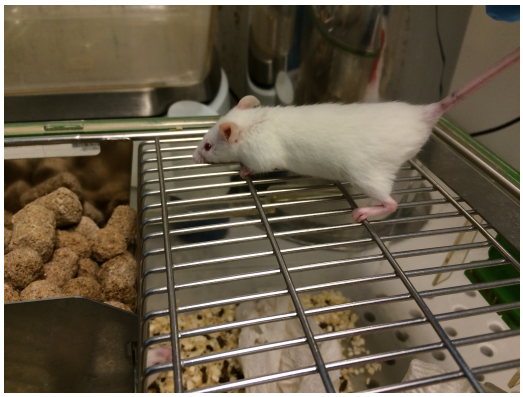

Figure. 2.3 – Image of a nod/scid mouse used in *in vivo* experiments.

When it comes to designing humane animal research studies, an accepted system is the implementation of the 3 R's, Replacement, Refinement & Reduction.

Replacement refers to methods that avoid using animals. The term includes absolute replacements (i.e., replacing animals with inanimate systems such as computer programs) as well as relative replacements (i.e., replacing animals such as vertebrates with cells).

Refinement refers to modifications of husbandry or experimental procedures to enhance animal wellbeing and minimize or eliminate pain and distress.

Reduction involves strategies for obtaining comparable levels of information from the use of fewer animals or for maximizing the information obtained from a given number of animals (without increasing pain or distress) so that in the long run fewer animals are needed to acquire the same scientific information (41).

2.11) MRI

The superior imaging modality MRI, with its excellent tissue contrast, is a risk-free procedure for the patients because it does not use ionizing radiation.

The source of the MRI signal is based on the hydrogen nuclei or protons, which are abundantly present in tissue. Each proton is positively charged, and is also constantly spinning around its own axis. According to physics theory, a moving electrical charge of this kind generates a current, which in turn creates a magnetic field.

The orientations of all these protons in tissue are usually randomly directed, creating a net magnetic moment, which is zero. However, when a biological specimen is placed within the magnet of an MRI system, the protons will align either parallel or anti-parallel with the main magnet field, B_0. The majority of protons will align parallel, as this requires the least energy. The difference between the number of protons aligned parallel and the number of protons aligned anti-parallel is usually very small. However, this difference increases with elevated magnetic field strength, and is the source for generating a signal, which in the end is reconstructed to become part of the MR image (42).

In order to detect a signal from the precessing protons, the protons need to be manipulated. Radiofrequency (RF) pulses are therefore switched on and off, knocking the protons out of the alignment with B_0. The disturbance occurs when energy with the same frequency as the precession frequency is applied to the tissue, causing resonance. The net magnetic moment will as a consequence move out of alignment with B_0, and the protons are moved into the transverse plane, or the x-y plane (42, 43).

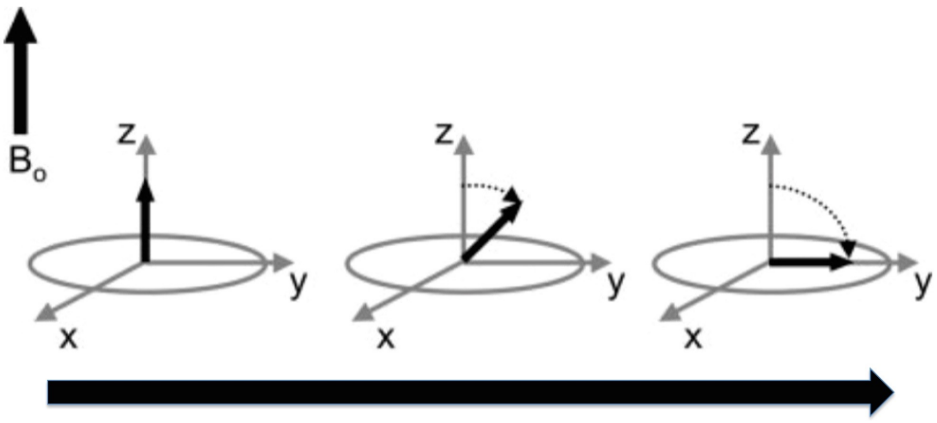

Figure. 2.4 – Absorption of RF energy, starting with the net magnetization, using a RF pulse at Larmor frequency energy is absorbed by the protons causing net magnetizations to rotate from z plane to x – y plane, adapted from (43).

The use of an RF pulse will move some of the protons from the parallel to the anti-parallel state, resulting in a reduction in overall longitudinal magnetism. Also the RF pulse makes the protons move in the same direction, or phase. The result is that a magnetization occurs in the transverse plane, moves at the Larmor frequency and thus generates an alternating voltage that can be detected in antennas or RF coils. The Larmor frequency is the sum magnetic field from these protons, which is now regarded a single vector M_0, rotates around B_0 with a precession frequency determined by the magnetic field. This signal is used in the formation of an MRI signal. When the RF pulse is turned off the protons will start to move out of phase and lose energy, termed «proton relaxation».

This takes place in two ways; transverse magnetism is referred to as T_2 or spin-spin relaxation, and longitudinal magnetism returns to the initial situation called T_1 or spin-lattice relaxation. The speed at which T_1 relaxation occurs is dependent on the properties of the surroundings. Therefore, different tissues or arrangements with hydrogen to other substances will produce different T_1 relaxation times. The time constant T_1 is the time it takes until longitudinal magnetism is regained to 63 % of its final value (Fig. a). T_2 relaxation describes loss of in-phase protons due to in homogeneities within the local tissue and within B_0. The time constant T_2 describes the time it takes before transverse magnetism is reduced to 37 % (Fig. b) (42, 43).

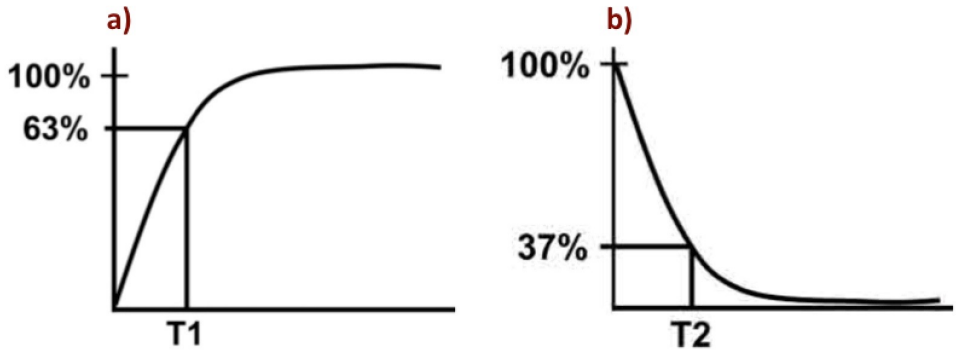

Fig. 2.5 – Representation of T1 and T2 curves. a) T1 characteristic of tissue, consisting of the time it takes for longitudinal magnetization to recover to 63%. b) T2 characteristic of tissue, consisting of the time it takes for transversal magnetization to decrease to 37%. Adapted from (43).

MRI studies were performed using a Bruker Biospec 7 Tesla (7 T) small animal scanner (Bruker BioSpin MRI, Ettlingen, Germany) equipped with a mouse head transmit/receive coil for transmit and a four channel mouse brain phased array for receive. Images were acquired using ParaVision 5.1 (Bruker BioSpin MRI). MRI was used to study tumor burden with and without drug in a nod/scid mouse after administration of the Omniscan contrast (GE Healthcare, Fairfield, CT, USA) as commonly used in the clinic.

3) Results

Prior to my arrival, animal models and drug selection had been established, with cMAP results represented in subsection 3.1. My task consisted of a preliminary *in vitro* drug screening with the application of possible candidates in *in vivo* trials, of the remaining 9 candidates.

3.1) cMAP and Drug Selection

After intracardiac injections, tumor burden was seen mainly in the animal brains, and to some extent in bone, adrenals and ovaries (Figs 3.1A, 3.1 B). Principal component analysis showed distinct clustering of the gene data obtained from the different organs (Fig 3.1 C). A bioinformatics analysis was performed, comparing differentially expressed genes in the brain metastatic cells, with gene expression in the metastatic cells from adrenals, bone and ovaries. From the analysis we could determine a list of 108 candidate genes (54 up, 54 down; Fig 3.1 D), potentially important in metastasis to the brain. This gene list was compared to gene profiles published online (Connectivity Map or cMap, Broad Institute, Boston, MA). In cMap, thousands of commonly used compounds and drugs have been tested on several different cancer cell lines, and gene profiles before and after treatment have been determined and published online (Fig 3.1 E). We found that 20 drugs published in cMap resulted in the exact opposite gene profile, compared to our gene profile. The top ten drugs were tested in Prof Thorsens lab prior to my arrival (Fig 3.1 F), if any of them showed efficiency *in vitro*, they continued to study *in vivo*. They found that **β-sitosterol effectively inhibited brain metastatic tumor cell growth *in vitro* and *in vivo***.

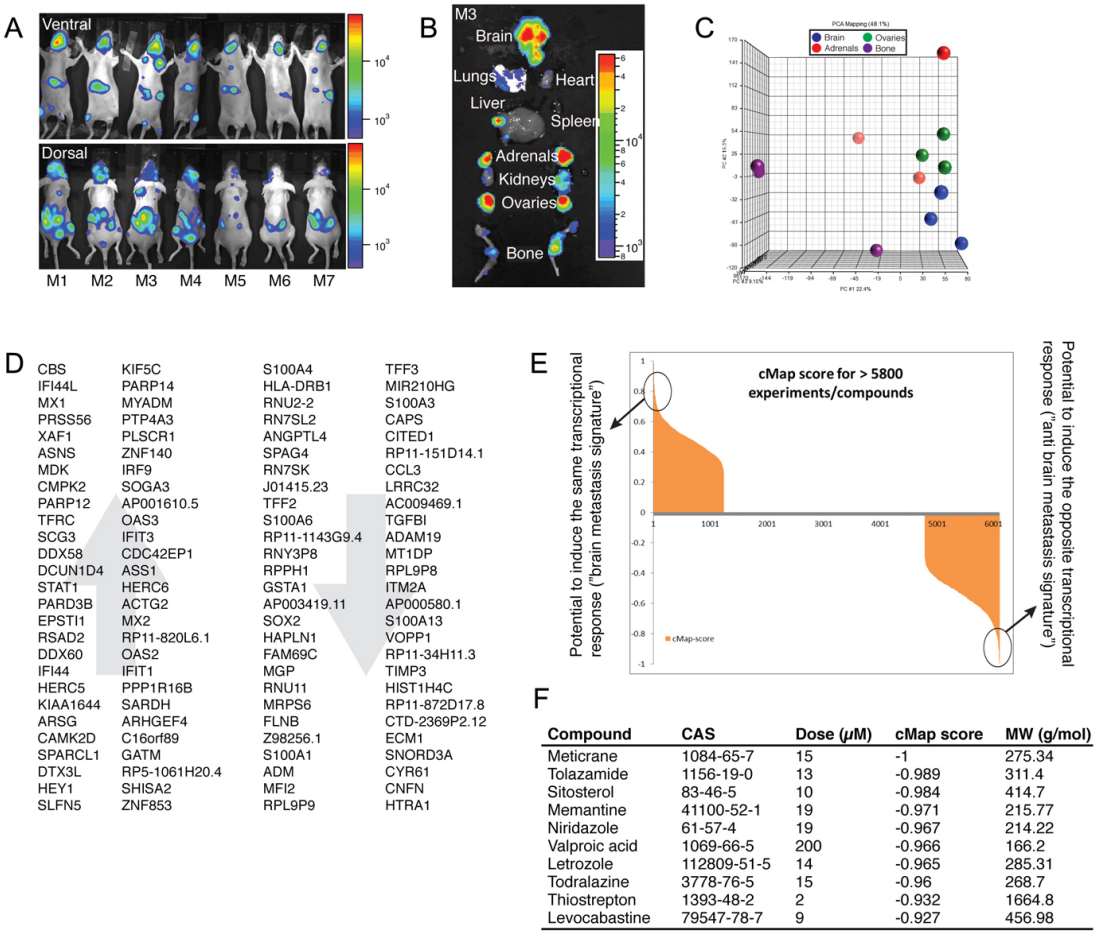

Compound	CAS	Dose (μM)	cMap score	MW (g/mol)
Meticrane	1084-65-7	15	-1	275.34
Tolazamide	1156-19-0	13	-0.989	311.4
Sitosterol	83-46-5	10	-0.984	414.7
Memantine	41100-52-1	19	-0.971	215.77
Niridazole	61-57-4	19	-0.967	214.22
Valproic acid	1069-66-5	200	-0.966	166.2
Letrozole	112809-51-5	14	-0.965	285.31
Todralazine	3778-76-5	15	-0.96	268.7
Thiostrepton	1393-48-2	2	-0.932	1664.8
Levocabastine	79547-78-7	9	-0.927	456.98

Figure. 3.1 Tissue sample generation, expression profiling, and Connectivity Map analysis. **A.** BLI at 5 weeks post injection of $5*10^5$ H1DL2 cells. **B.** Detailed mapping of organ involvement by ex vivo BLI. **C.** Principal components analysis of all replicates (brain-blue, ovaries-green, adrenals-red, bone-purple). **D.** The brain metastasis gene signature with the left two panels showing 54 genes that were upregulated in brain metastases and the right two panels showing 54 genes that were downregulated in brain metastases. **E.** Query results from the cMap database using the 108-gene signature. A score of <0 to –1 means net reversal of the signature (negative correlation) and a score of >0 to +1 means net induction of the signature (positive correlation). **F.** Top 10 compounds from the Connectivity Map (cMap) analysis with the potential to induce the opposite transcriptional response to the brain metastasis signature ("anti brain metastasis signature"). Chemical abstracts service (CAS) registry numbers, reported dose tested, cMap score, and molecular weight (MW) are provided.

3.2) *In Vitro* Studies

3.2.1) Monolayer Viability Assay

The monolayer viability assay was used to study cell viability based on Resazurin reduction as described in chapter 1.7.1. The experiments were done for all the four cell lines, using the same drug concentrations and the same observation time.

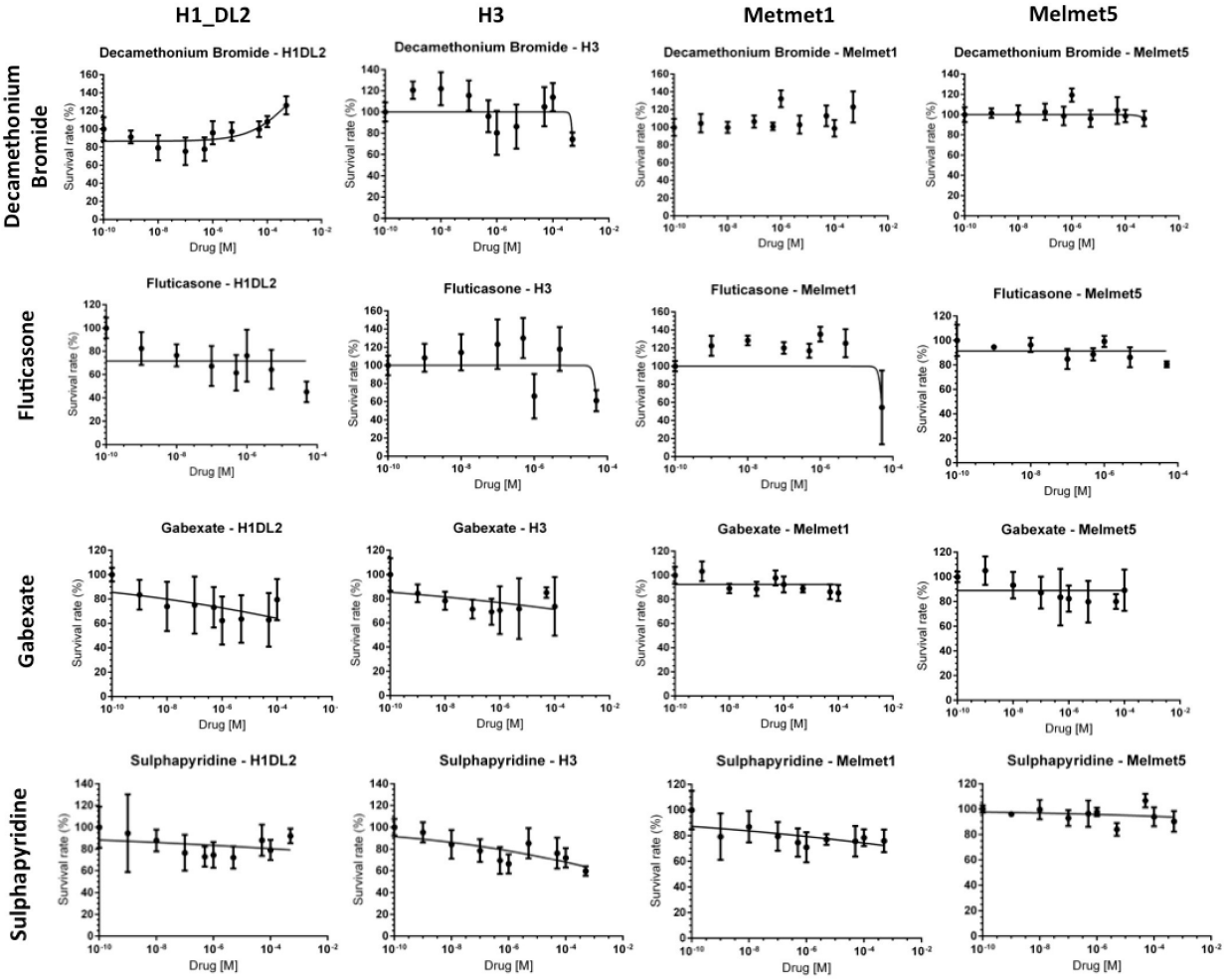

Figure 3.2 - Monolayer proliferation assay for Decamethonium Bromide, Fluticasone, Gabexate and Sulphapyridine in all cell lines. The cells were treated with different concentrations of the drugs to study the possible inhibitory effect on the proliferation capacity of these tumor cells. The experiment was replicated 3 times under the same conditions.

As shown in figure 3.1, the drug-response plots used to determine the inhibitory effects of Decamethonium Bromide, Fluticasone, Gabexate and Sulphapyridine on the viability of the cell lines, showed almost linear graphs, regardless of drug concentration. In other words, these three drugs did not affect cell viability.

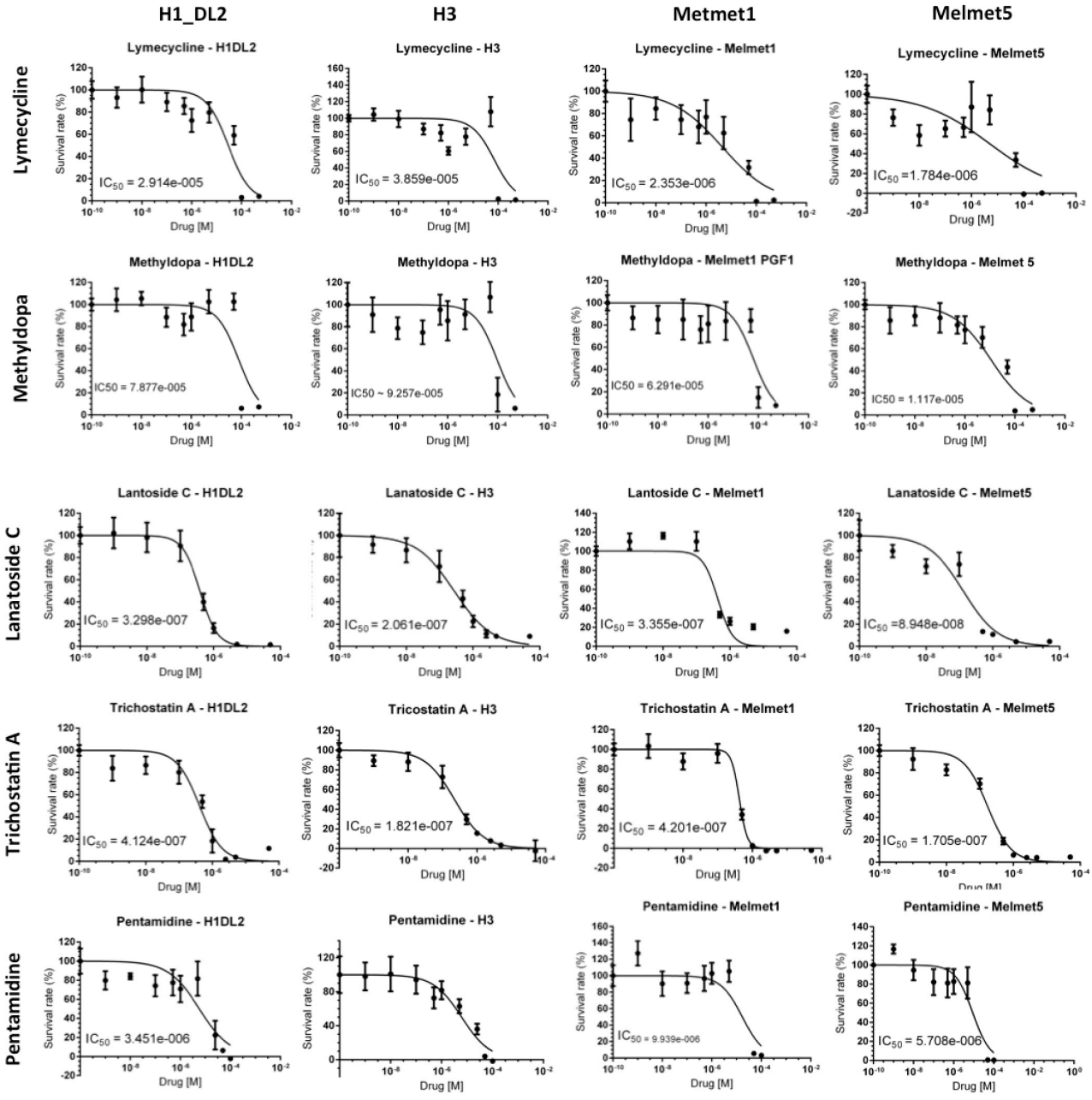

Figure 3.3 - Monolayer Viability assay for Lymecycline, Methyldopa, Lanatoside C, Trichostatin A and Pentamidine in all cell lines. The cells were treated with different concentrations of the drugs to study the possible inhibitory effect on the proliferation capacity of these tumor cells. Experiment was replicated 3 times under the same conditions.

As shown in figure 3.2, the drug-response plots, used to determine the inhibitory effects of all represented drugs on the viability of the cell lines, ,showed a sigmoidal shape. The percentage of relative viability (Y-axis) was plotted as a function of the logarithmic drug concentration (X-axis) for all four cell lines. The required dose of Lymecycline and Methyldopa for 50% inhibition (IC_{50}) of the cell viability was in the 10^{-5} range, followed by Pentamidine with 10^{-6}, the Trichostatin A and Lanatoside C with 10^{-7}. A table containing all IC_{50} values is found in chapter 3.3. Drug doses below the IC_{50} value did not have a statistical significant inhibitory effect. In our experiments, a sufficient range of drug concentrations were chosen to ensure that there were enough points below and above the IC_{50} dose, thereby ensuring that a proper curve fit could be made.

The relatively flat slope of a dose response curves below the IC_{50} dose suggest that the effect on viability in this dose range was minimal.

3.2.2) Soft Agar proliferation

The soft agar assay was employed to study spheroid development of melanoma brain cells in presence and absence of treatment. Cells were cultured in soft agar, and developed into spheroids during a time period of up to 14 days.

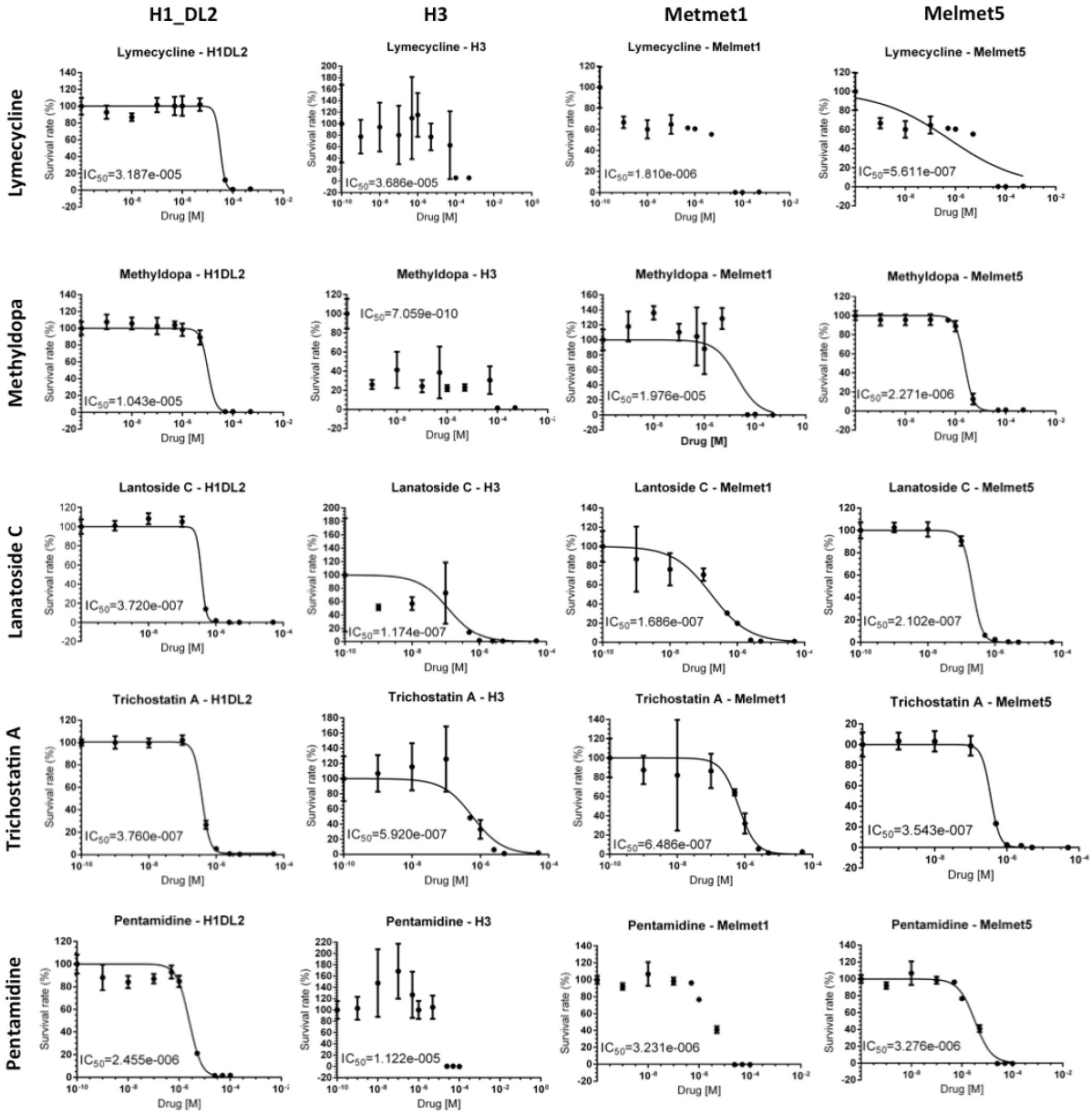

Figure 3.4 – Soft agar proliferation assay for Lymecycline, Methyldopa, Lanatoside C, Trichostatin A and Pentamidine. The cells were treated with different concentrations of the drugs to study the possible inhibitory effect on the proliferation capacity of these tumor cells. Experiment was replicated 3 times under the same conditions. Curve fits not possible in all samples.

Only the drugs that showed decrease in cellular viability in the Monolayer proliferation assay were screened utilizing this assay: Lymecycline, Methyldopa, Lanatoside C, Trichostatin A and Pentamidine.

All five drugs showed an inhibitory effect on tumor cells grown in the 3D agar assay. The survival curves for Lymecycline cells, first row in figure 3.4, showed that the required doses for 50% maximal inhibitory (IC_{50}) differed between all cell lines, ranging between 10^{-5}M and 10^{-7}M. When using Methyldopa (second row in figure 3.4), the required doses for 50% maximal inhibitory (IC_{50}) ranged between 10^{-5}M and 10^{-10}M. The results showed that this drug is very effective on the H3 cell line.

Both Lanatoside C and Trichostatin A, row three and four respectively in figure 3.4 showed that the required doses for 50% maximal inhibitory (IC_{50}) was constant between all cell lines requiring a concentration in the 10^{-7}M region, to negatively affect the viability. Finally Pentamidine (fifth row of figure 3.4), showed that the required doses for 50% maximal inhibitory (IC_{50}) was constant for 3 cell lines, H1_DL2, Melmet1 and Melmet 5 requiring a concentration in the 10^{-6}M region. The IC_{50} dose for the H3 cell line was 10^{-5} M.

When concentrations higher than the IC_{50} doses were administered to the cells, this affected the cells considerably, as they showed lower capacity to reduce Resazurin to resorufin, indicating decreased number of viable cells. A table containing all IC_{50} values is shown in chapter 3.3.

3.2.3) Summary of all IC_{50} Results

Table 3.5 shows all the IC50 doses obtained for the monolayer assay and the soft agar assay. Each result is mean value ± SD of three experiments. The results show that Lanatoside C and Trichostatin A were the most effective drugs, followed by Pentamidine. Reliable values for the IC_{50} doses could not be obtained for Decamethonium Bromide, Sulphapyridine, Fluticasone and Gabexate, as these drugs affected cell viability only minimally.

Table 3.1 – Table containing IC_{50} values for all *In vitro* studies.

IC50 Dose	Monolayer Assay				Soft Agar Assay			
	H1_DL2	H3	Melmet1 pGF1	Melmet5 pGF1	H1_DL2	H3	Melmet1 pGF1	Melmet5 pGF1
Pentamidine	1.70E-05	1.07E-05	1.18E-05	1.32E-05	2.41E-06	1.12E-05	1.87E-06	3.56E-06
Methyldopa	6.93E-05	1.05E-04	5.30E-05	2.38E-05	7.89E-06	1.10E-05	1.29E-05	2.36E-06
Trichostatin A	1.58E-06	2.00E-07	2.47E-07	1.76E-07	3.60E-07	7.66E-07	7.66E-07	3.71E-07
Lanatoside C	2.90E-07	2.08E-07	3.31E-07	2.07E-07	2.50E-07	1.85E-07	3.48E-07	2.11E-07
Lymecycline	2.99E-05	4.91E-05	3.33E-01	2.30E-05	2.59E-05	3.63E-05	1.42E-05	2.21E-05
Decamethonium Bromide	-	-	-	-	-	-	-	-
Sulphapyridine	-	-	-	-	-	-	-	-
Fluticasone	-	-	-	-	-	-	-	-
Gabexate	-	-	-	-	-	-	-	-

3.2.4 DNA Cell Cycle Analysis

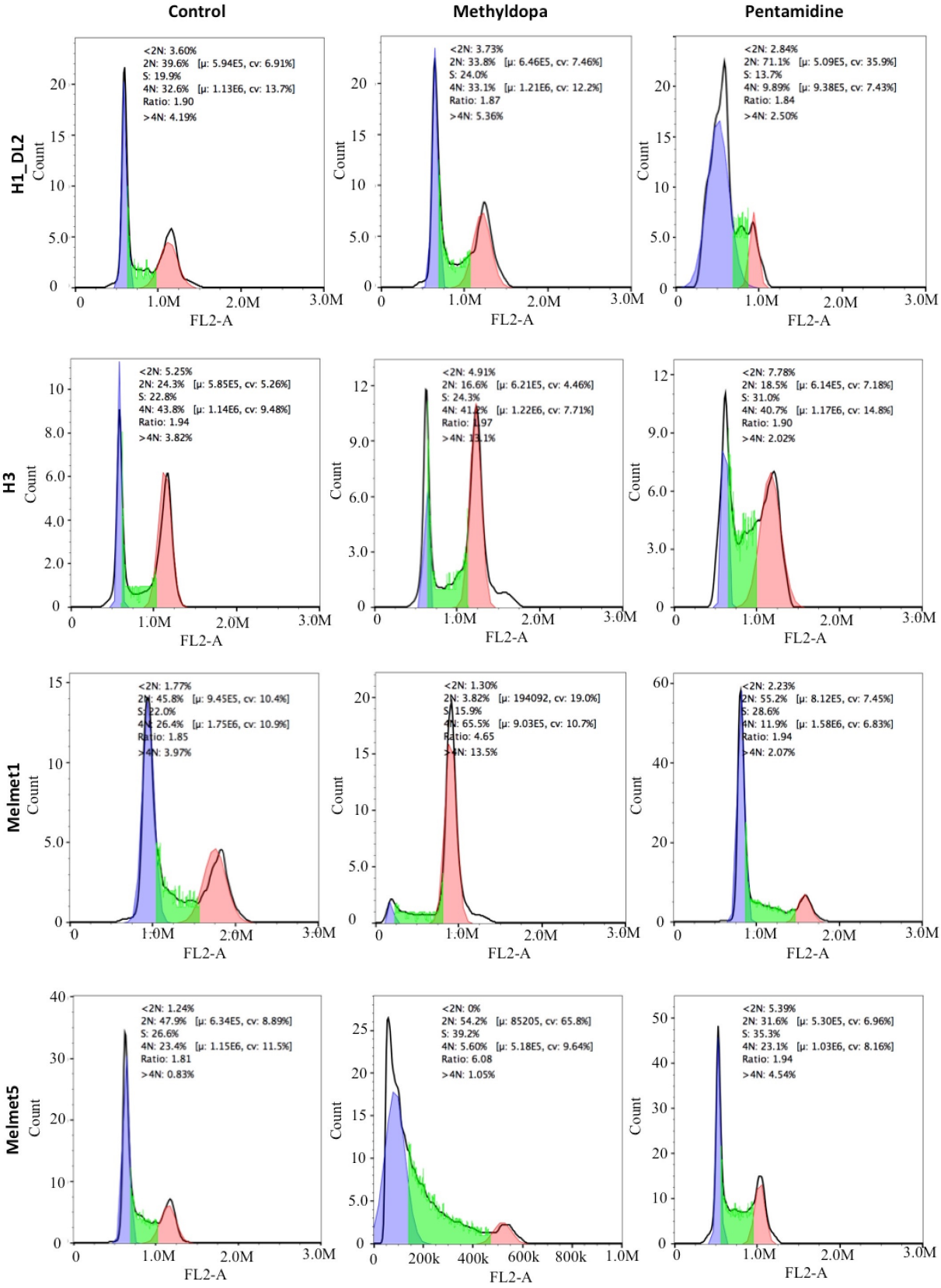

Figure 3.5 - Cell cycle analysis of H1_DL2, H3, Melmet1 pGF1, and Melmet5 pGF1 by flow cytometry. Cell cycle phases in the histograms represented above are color coordinated, where the purple color is the estimated G1 phase, the green color is the estimated S phase, and the red color is the estimated G2 phase. We considered <2N along with 2N as G_1 phase, and 4N along with >4N as G_2/M phase. Histogram presents axis of FL2-A vs. Count, that represents number of events able to pass FL2 filter, which is a PMT (photomultiplier tube) detector that allows wavelengths between 565 and 605nm to pass through.

Flow cytometry was employed to study the effects of drug on the cell cycle of the different cell lines. Triple experiments were performed on all cell lines, using 100mM of Methyldopa or Pentamidine. Untreated cells were used as negative controls. We did not perform flow cytometry using Lymecycline or Lanatoside C, as these drugs are too large to cross an intact blood-brain barrier, and therefore were excluded from further *in vivo* experiments. Trichostatin A was also excluded from this analysis, as *in vivo* experiments (which were done before we did the DNA analysis) showed no drug effects on the brain tumors in animals.

When H1_DL2 cells (figure 3.6 first row) were treated with Methyldopa we noticed a broadened G_2/M phase whereas when treated with Pentamidine the G_1 phase was broadened and S phase slightly arrested. With the H3 cells (figure 3.6 second row) there was a significant increase in G_2/M phase with both drugs with the addition of a broadened S phase with Pentamidine. Both drugs had a severe effect on Melmet 1 (Figure 3.6 third row) with an arrest of the G_1 and S phase and a significant increase in the G_2/M phase once treated with Methyldopa. Whilst when treated with Pentamidine we observe a broadened G_2/M phase and an arrested G_1 phase. Melmet 5 (figure 3.6 forth row) once treated with Methyldopa it was clear to see that G_1 and S phase broadened with an arrest in the G_2/M Phase. Meanwhile when treated with Pentamidine no significant phase shift was verified apart from a slightly higher accumulation in the G_2/M region.

Table 3.6 shows all the values in percentage of each cell cycle phase, for each cell line and the two drugs used. Each result is mean value ± SD of three experiments. The results as explained above clearly show phase shift within all treatments but, statistically the most relevant shift if found when H1_DL2 is treated with Pentamidine. Here we can evidently see a reduction in the G_2/M phase.

Table 3.2 – Statistical information relative to cell cycle analysis, mean values ± SD of the whole experiment. ns = not significant (P > 0.05); * = P ≤ 0.05; ** = P ≤ 0.01; *** = P ≤ 0.001; **** = P ≤ 0.0001.

	Untreated			Methyldopa			Pentamidine		
(%)	G1	S	G2/M	G1	S	G2/M	G1	S	G2/M
H1_DL2	46,10±4,09	17,55±3,32	36,33±0,66	38,83±1,83	20,40±5,09	40,83±3,33	63,65±14,50	20,80±10,04	16,00±5,10*
H3	31,31±2,48	24,80±2,83	43,90±5,27	19,46±2,90	32,75±11,95	47,63±9,44	34,05±10,99	19,46±16,32	46,42±4,97
Melmet1_pGF1	46,08±2,11	25,85±5,44	28,09±3,23	26,08±29,64	27,05±15,77	46,87±45,45	55,43±2,84	25,35±4,60	19,25±7,47
Melmet5_pGF1	45,98±4,47	26,90±0,42	27,08±4,01	52,55±2,33	26,95±17,32	20,58±19,69	40,75±5,31	34,15±1,63	25,11±3,59

3.2.5) Apoptosis assay

A colorimetric method was used to determine potential changes in apoptosis for the four cell lines after treatment with Pentamidine and Methyldopa. We did not perform the apoptosis assay using Lymecycline, Lanatoside C and Trichostatin A, for the same reasons as explained in Section 3.3

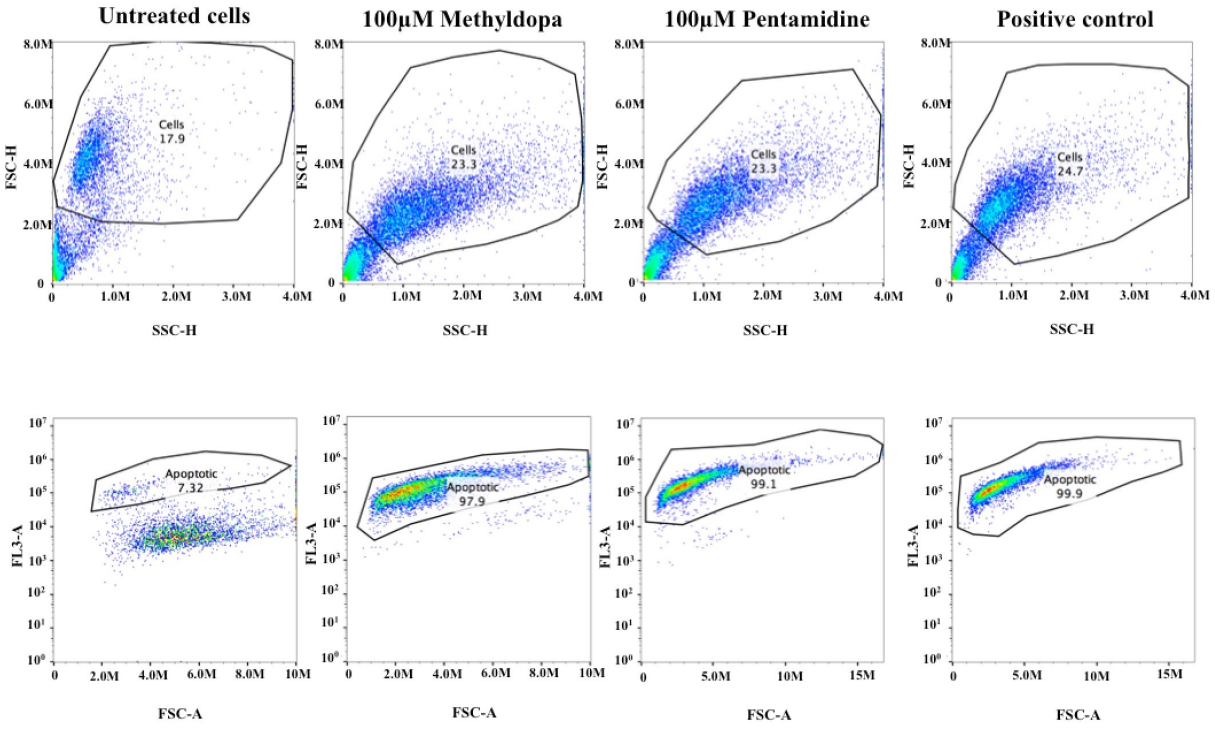

Figure 3.6 – Apoptosis assay on H1_DL2 human melanoma metastasis cell line. Represented above (first row) is a linear forward-scatter vs. side-scatter plot (FSC-H vs. SSC-H). FSC gives us information relative to the size of healthy/dead cell whilst, SSC informs us about cell fluorescence and granularity. It can be inferred that a rough cell such as a cell undergoing apoptosis would have high side scatter signals. These cytograms display both cells and cell debris, cell of interest are gated excluding debris. The second row shows FL3-A vs. FSC-H cytograms (FL3 channel used to detect rose bengal fluorescence); show gated cells from row above. We can clearly see two cell populations, as distinguished by the vertical axes. The upper populations are the apoptotic cells, since they express more color. Apoptotic cells were then gated giving us a total value in percentage.

For untreated H1_DL2 cells, 7.3% of the cells were apoptotic. When treated with 100 µM Methyldopa, around 98% of all cells were apoptotic, while around 99% of the cells were apoptotic after treatment with 100mM Pentamidine (Figure 3.7, Table 3.11).

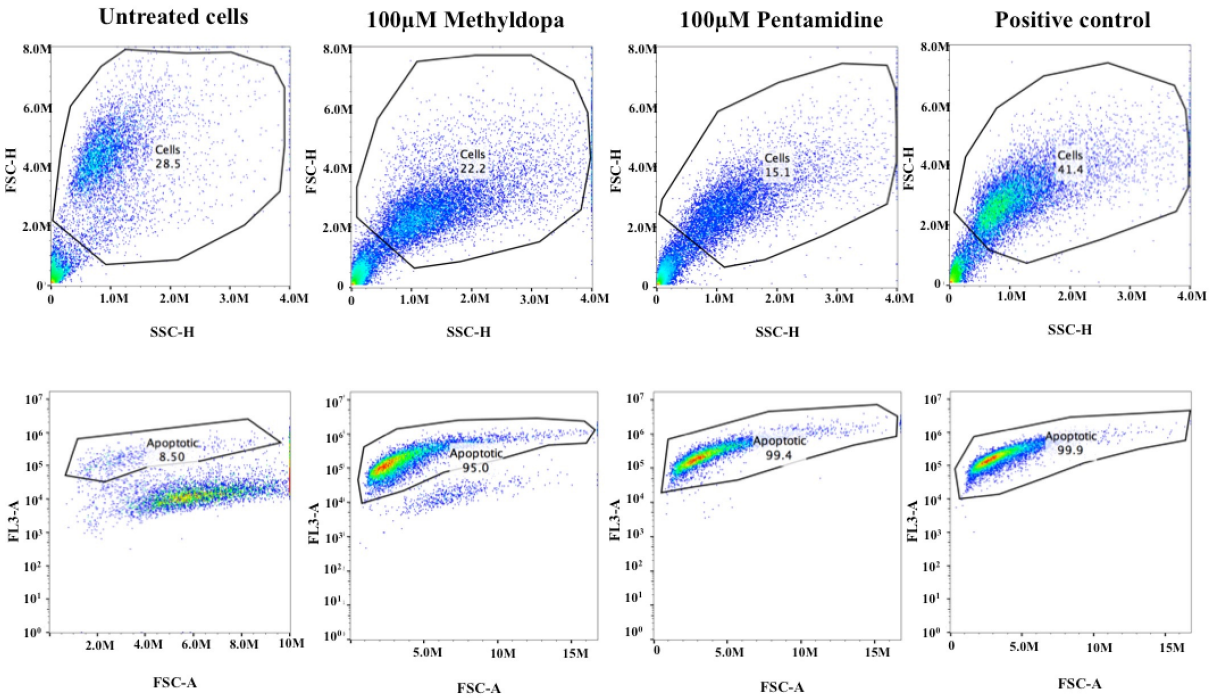

Figure 3.7 – Apoptosis assay on H3 human melanoma metastasis cell line. Represented above (first row) is a linear forward-scatter vs. side-scatter plot (FSC-H vs. SSC-H). FSC gives us information relative to the size of healthy/dead cell whilst, SSC informs us about cell fluorescence and granularity. It can be inferred that a rough cell such as a cell undergoing apoptosis would have high side scatter signals. These cytograms display both cells and cell debris, cell of interest are gated excluding debris. The second row shows FL3-A vs. FSC-H cytograms (FL3 channel used to detect rose bengal fluorescence); show gated cells from row above. We can clearly see two cell populations, as distinguished by the vertical axes. The upper populations are the apoptotic cells, since they express more color. Apoptotic cells were then gated giving us a total value in percentage.

For the H3 cell line, untreated cell populations contained 8.5% apoptotic cells, and in cells treated with Pentamidine around 99% of the cells were apoptotic. After Methyldopa treatment, approximately 95% were apoptotic (Figure 3.8, Table 3.11).

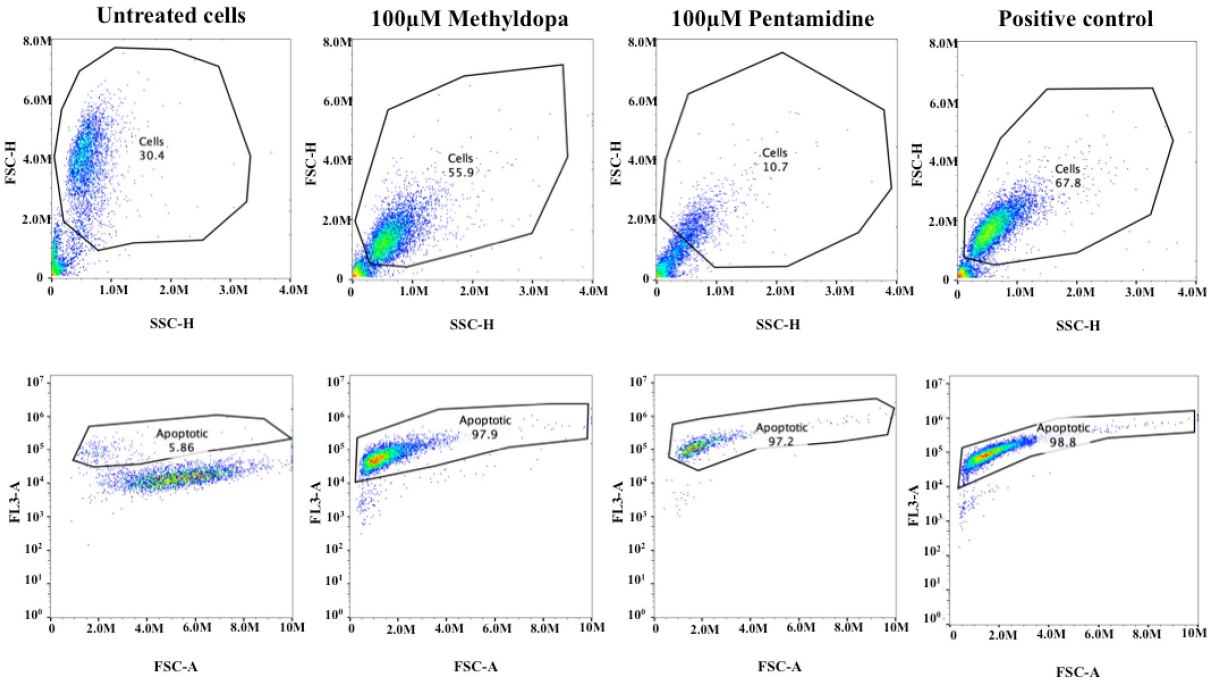

Figure 3.8 – Apoptosis assay Melmet1_pGF1 human melanoma metastasis cell line. Represented above (first row) is a linear forward-scatter vs. side-scatter plot (FSC-H vs. SSC-H). FSC gives us information relative to the size of healthy/dead cell whilst, SSC informs us about cell fluorescence and granularity. It can be inferred that a rough cell such as a cell undergoing apoptosis would have high side scatter signals. These cytograms display both cells and cell debris, cell of interest are gated excluding debris. The second row shows FL3-A vs. FSC-H cytograms (FL3 channel used to detect rose bengal fluorescence); show gated cells from row above. We can clearly see two cell populations, as distinguished by the vertical axes. The upper populations are the apoptotic cells, since they express more color. Apoptotic cells were then gated giving us a total value in percentage.

For the untreated Melmet 1 cell line, approximately 6% were apoptotic. After treatment with Pentamidine around 98% of the cells showed apoptosis. Around 97% of the cells were apoptotic after treatment with Methyldopa (Figure 3.9, Table 3.11).

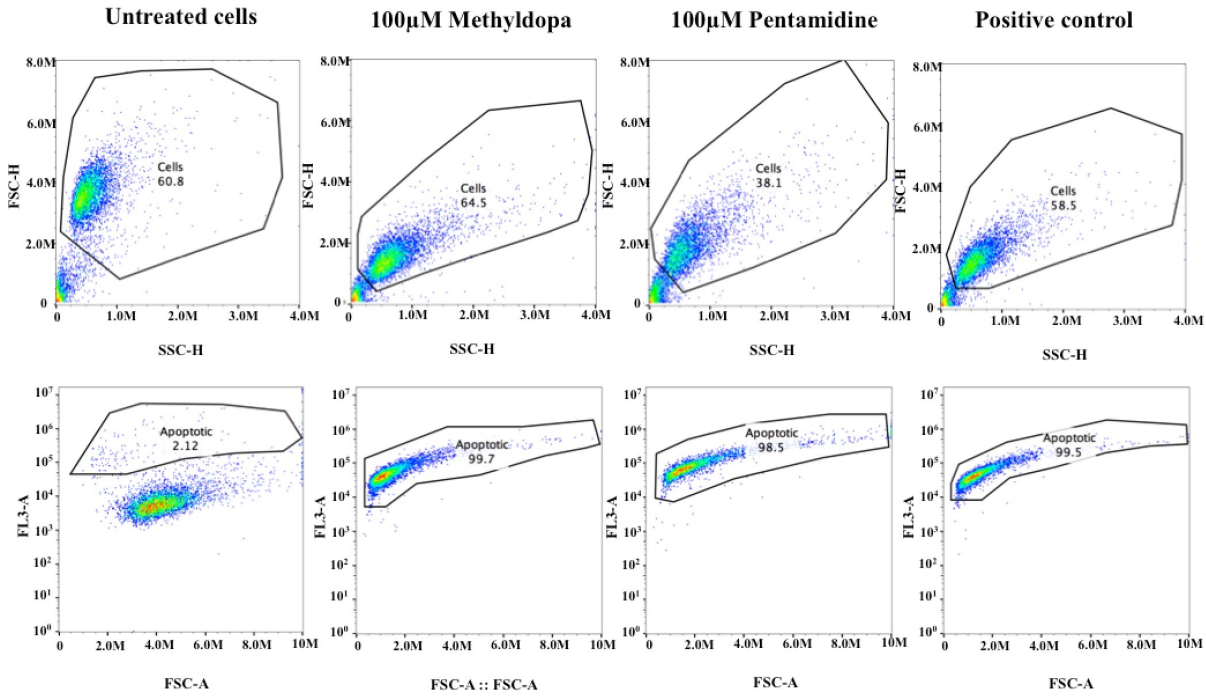

Figure 3.9 – Apoptosis assay on Melmet5_pGF1 human melanoma metastasis cell line. Represented above (first row) are linear forward-scatter vs. side-scatter plots (FSC-H vs. SSC-H). FSC gives us information relative to the size of healthy/dead cell whilst, SSC informs us about cell fluorescence and granularity. It can be inferred that a rough cell such as a cell undergoing apoptosis would have high side scatter signals. These cytograms show both cells and cell debris, cell of interest are gated excluding debris. The second row shows FL3-A vs. FSC-H cytograms (FL3 channel used to detect rose bengal fluorescence); show gated cells from row above. We can clearly see two cell populations, as distinguished by the vertical axes. The upper populations are the apoptotic cells, since they express more color. Apoptotic cells were then gated giving us a total value in percentage.

Untreated Melmet 5 cells had approximately 2.5 ± 0.6 % apoptotic cells, after Pentamidine treatment around 98.6% of the cells were apoptotic, and after Methyldopa treatment approximately 99.5% were apoptotic (Figure 3.10, Table 3.11).

Table. 3.3 – Percentage of apoptotic cells for untreated cells, and cells treated with 100mM Pentamidine or 100mM Methyldopa. As positive controls, cells were treated with 10mM H_2O_2. The results shown are mean values of 3 experiments ± standard deviation. ns = not significant ($P > 0.05$); * = $P \leq 0.05$; ** = $P \leq 0.01$; *** = $P \leq 0.001$; **** = $P \leq 0.0001$.

Cell Line	Untreated [%]	Pentamidine [%]	Methyldopa [%]	Positive Control [%]
H1_DL2	7.4 ± 1.8	99.1 ± 0.3****	97.8 ± 0.5****	99.7 ± 0.5****
H3	8.2 ± 0.2	95.5 ± 0.6****	94.5 ± 0.6****	99.9 ± 0.1****
Melmet 1	5.5 ± 2.7	98.1 ± 0.8****	97.1 ± 2.3****	98.9 ± 0.1****
Melmet 5	2.5 ± 0.6	98.6 ± 0.2****	99.5 ± 0.2****	99.7 ± 0.3****

3.3) *In Vivo* Studies

3.3.1) Experimental Layout

Three drugs were tested *In Vivo,* (Trichostatin A, Methyldopa and Pentamidine). Drug selection was based on *In Vitro* results and molecular weight to have a higher change of crossing the BBB.

3.3.2) In vivo Trichostatin A (TSA) treatment

The first animal experiment was performed to determine the potential *in vivo* effects of Trichostatin A. The National Animal Research Authority approved all animal procedures. Twelve weeks old female nod/scid mice were injected with $1 \cdot 10^6$ H1_DL2 cells in the left cardiac ventricle.

Treatment then began the following day; animals were subdivided into 2 groups, one control group (no treatment, n = 8 animals), and one treatment group (1 mg/kg TSA, n = 8 animals). Treatment groups received intraperitoneal injections three times a week of the drug at a dosage of 1mg/kg. The animals were then kept in the animal facility under standard conditions; being fed a standard pellet diet and provided water *ad libitum*.

All groups were monitored daily and weighed 3 times per week to ensure the animals wellbeing, and to terminate the experiment within parameters of that which are humane (humane endpoints).

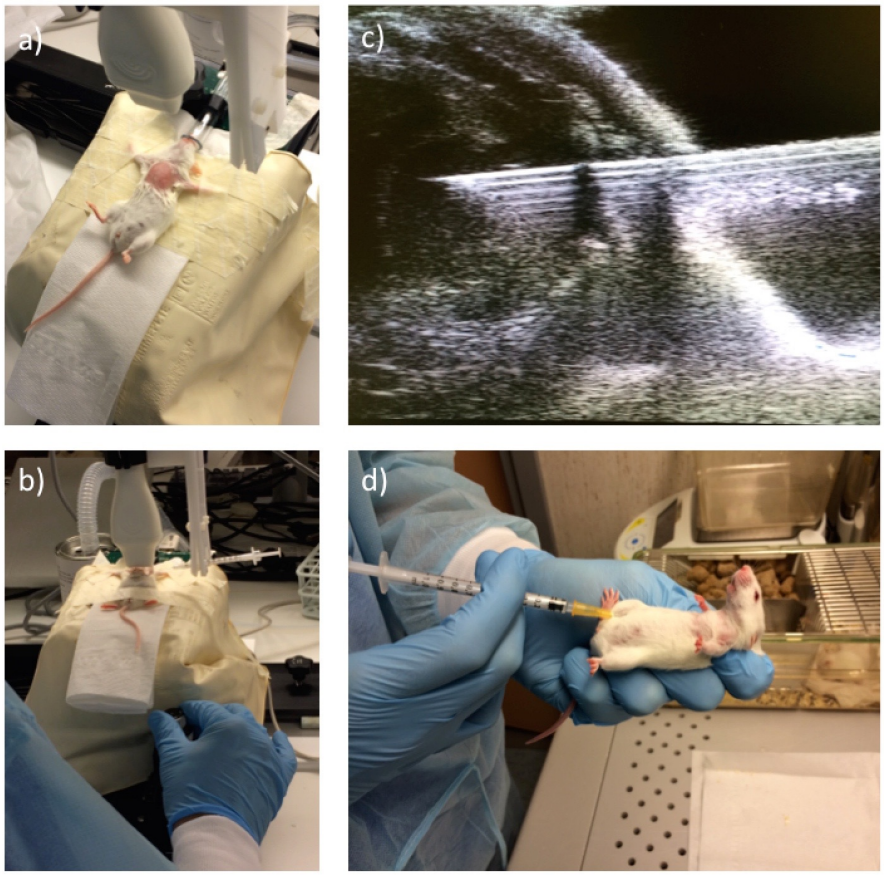

Figure. 3.10 – Illustration of intercardiac injection and interperitoneal treatment. Injection of tumor cells into the left cardiac ventricle of nod/scid mice (a). Ultrasound guided injection to left cardiac ventricle (b;c). Drug treatment consisting of intraperitoneal injections (d).

3.3.3) In vivo Pentamidine and Methyldopa treatment

In a second animal experiment, the two remaining drug candidates, as determined by the *in vitro* screening (Methyldopa and Pentamidine) were tested for *in vivo* efficacy. The National Animal Research Authority approved all animal procedures. Twelve weeks old female nod/scid mice were injected with $5 \cdot 10^5$ H1_DL2 cells in the left cardiac ventricle. Treatment then began the following day; the animals were subdivided in 3 separate groups with each group containing 4 animals. The first group was a control group, which received no treatment. The second group received intraperitoneal injections three times a week of Methyldopa dissolved in PBS at a dose of 20mg/kg. The third group received intraperitoneal injections 5 times a week of Pentamidine dissolved in PBS at a dose of 10mg/kg. The animals were then kept in the animal facility under standard conditions; being fed a standard pellet

diet and provided water *ad libitum*. All groups were monitored daily and weighed 3 times a week to ensure the animals wellbeing, and to terminate the experiment within parameters of which is humane (humane endpoints).

3.3.4) *In vivo* TSA

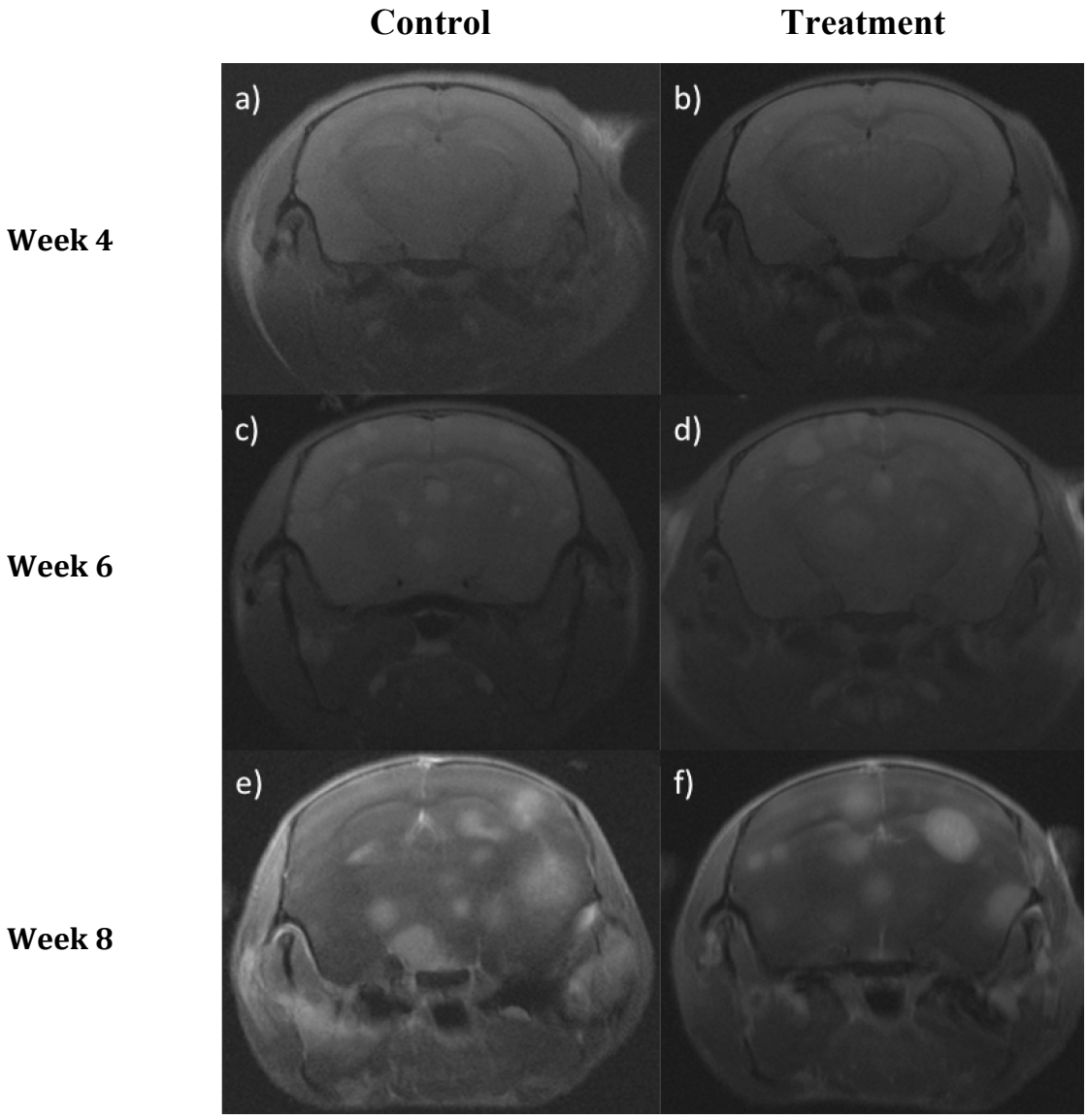

Figure. 3.11 - Representative MRI Scans of mice brains during TSA *In vivo* treatment over the period of the experiment. T1 scans after administering contrast were used to qualify tumor burden and volume. In these images its clear to see tumor establishment and progression throughout the experiment. Lighter white areas are tumors, which are emphasized due to uptake of the contrast agent Images **a, c** and **e** – Control animals over a period of 4, 6 and 8 weeks respectively. Images **b**, **d** and **f** – Animals treated with 1 mg/kg of TSA over a period of 4, 6 and 8 weeks respectively. As can be visualized tumor burden increases with the passing of time in both control and treatment mice, although this is much more apparent when treated with TSA.

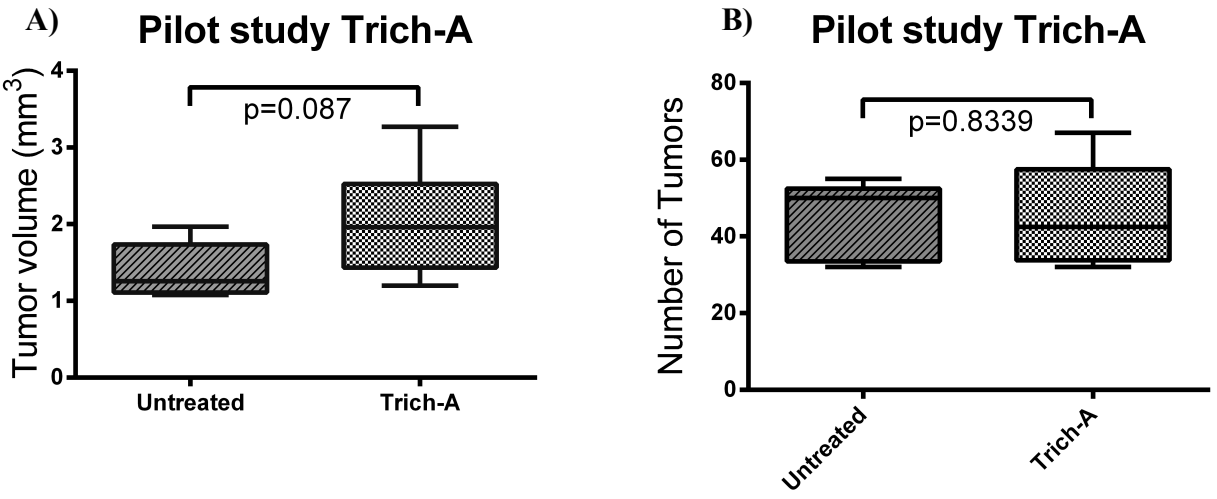

Figure. 3.12 – Graph representing tumor burden and volume during treatment at week 8. **A)** Tumor volume in untreated and treated animals. **B)** Tumor burden in untreated and treated animals. As is visualized both tumor volume and burden has a tendency to be increased in treated animals although not statistically significant.

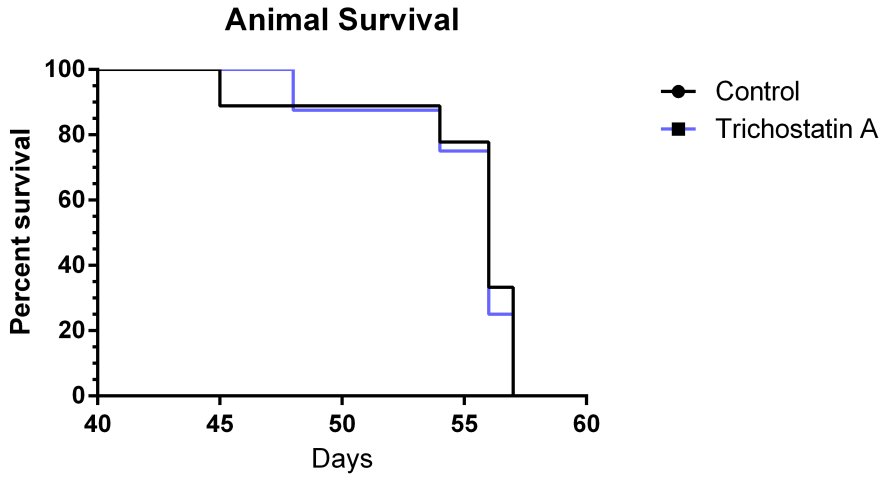

Figure. 3.13 – Graphic illustrating animal survival thought the course of the experiment. Both control and treatment animals had a very similar survival rate, no increase when treated with TSA.

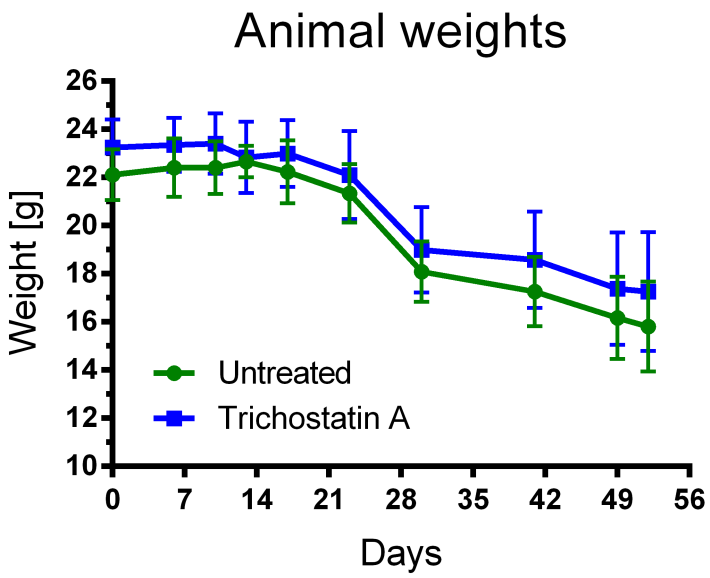

Figure. 3.14 – Graphic illustrating animal weights thought the course of the experiment. Graph shows animal weights declining throughout the experiment, with both groups weight declining at a similar ration, TSA group maintained relatively good weight until the end of the experiment.

In vivo experiments using TSA proved inefficient, tumor burden was maintained very similar to control animals. Mice treated with TSA had larger tumors in comparison to control animals and this is very clear in (Figure 3.12). Treated animals did not loose as much weight as control animals, but nothing significant and all in all animal survival was not affected.

3.3.5) *In vivo* Pentamidine/Methyldopa

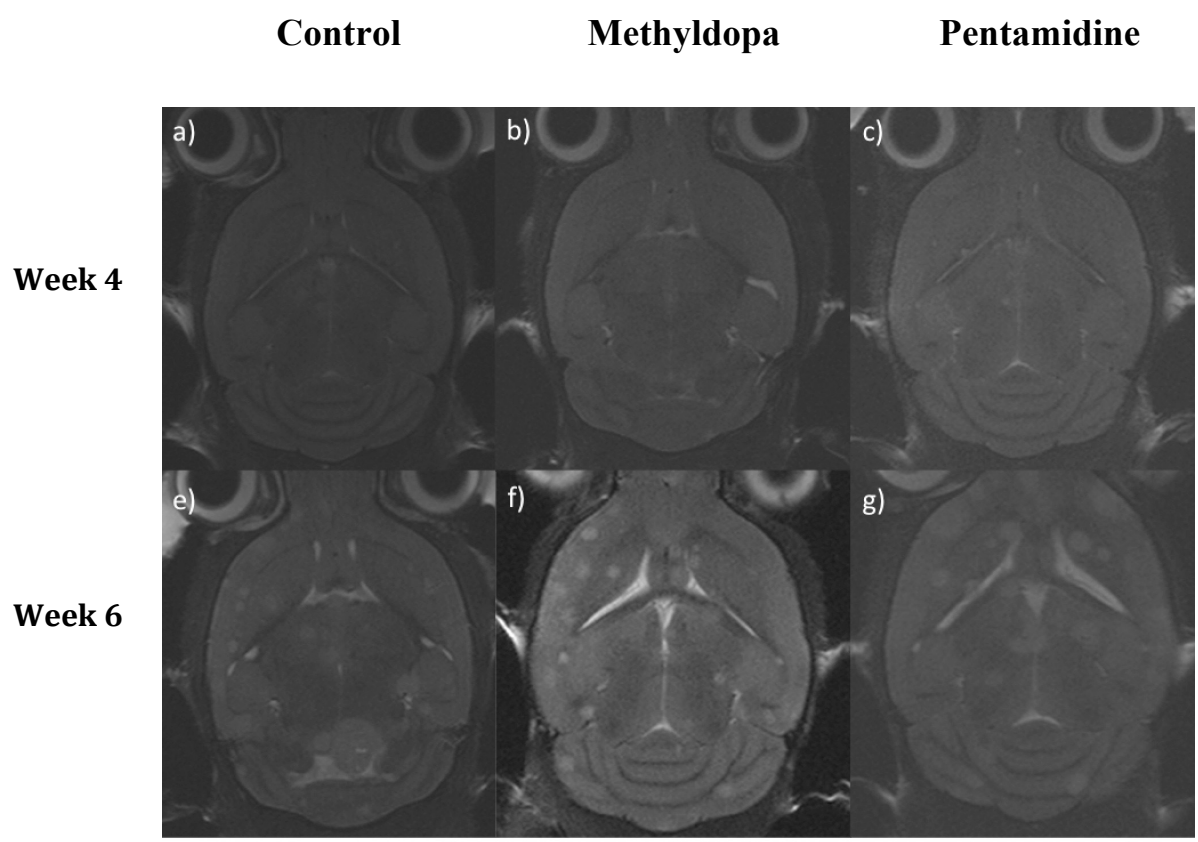

Figure. 3.15 - Representative MRI Scans of mice brains during Methyldopa/Pentamidine *in vivo* treatment over the period of the experiment. T1 scans after administering contrast were used to qualify tumor burden and volume. In these images its clear to see tumor establishment and progression throughout the experiment. Lighter white areas are tumors, which are emphasized due to uptake of the contrast agent. . Images **b** and **f** – Animals treated with 20 mg/kg of Methyldopa over a period of 4 to 6 weeks respectively. Images **c** and **g** – Animals treated with 10 mg/kg of Pentamidine over a period of 4 to 6 weeks respectively. As can be visualized tumor burden increases with the passing of time in both control and treated mice.

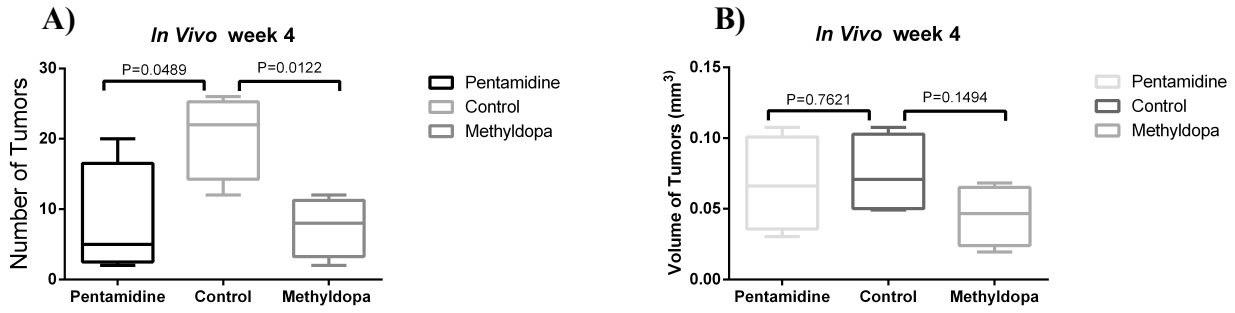

Figure. 3.16 – Graph representing tumor burden and volume during treatment at week 4. **A)** Number of tumors in untreated and treated animals. **B)** Tumor volume in untreated and treated animals. Number of tumors is greater in control animals followed by Pentamidine, with methyldopa showing promising results. The same is verified with tumor volume.

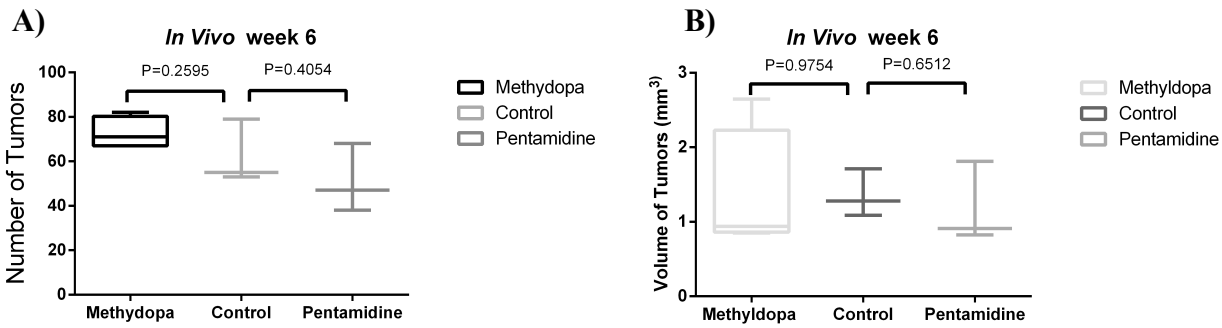

Figure. 3.17 – Graph representing tumor burden and volume during treatment at week 6. **A)** Tumor burden in untreated and treated animals. **B)** Tumor volume in untreated and treated animals. The results here show that at week 6 none of the drugs had promising effects on tumor burden and volume.

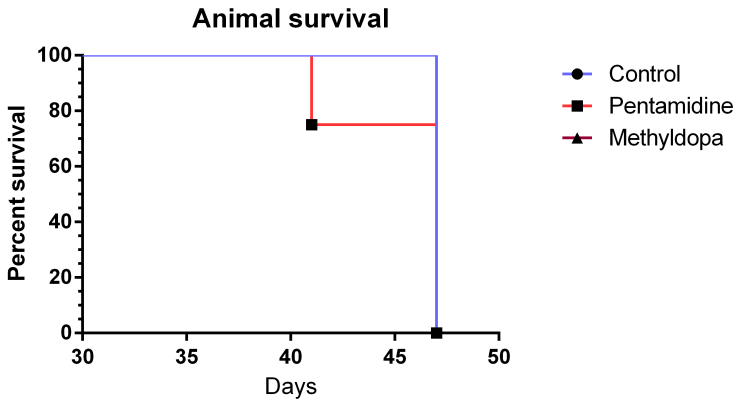

Figure. 3.18 – Graphic illustrating animal survival through the course of the experiment. As seen in the graph, 1 animal of the Pentamidine treatment group was euthanized around day 41, with all the remaining animals euthanized at day 47 terminating the experiment, to ensure wellbeing and minimize animal suffering (humane endpoints).

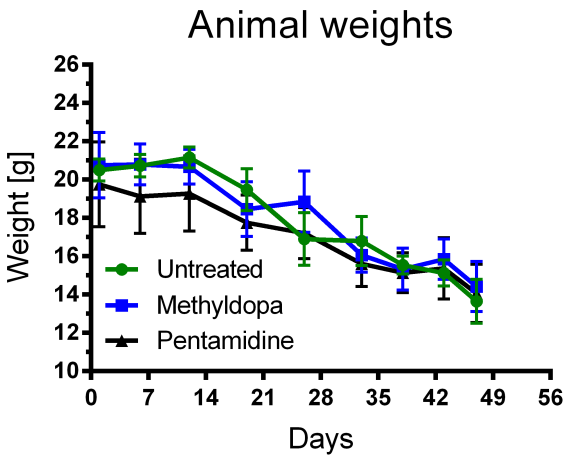

Figure. 3.19 – Graphic illustrating animal weights throughout the course of the experiment. Graph shows animal weights declining throughout the experiment, with a gain of weight in methyldopa treated animals around week 4.

In Vivo experiments using Pentamidine proved inefficient, tumor burden maintained very similar to control animals. Mice treated with this drug had similar results as control animals throughout the experiment (week 4 and 6) and this is clear in figures represented above. Treated animals lost a lot of weight in the beginning of the experiment but other

groups caught up. This group's survival was worse than the control and methyldopa group with the loss of one animal around day 41.

In vivo experiments using Methyldopa proved efficient, in an early stage. A transient effect was verified around week 4, with less and smaller tumors in comparison to the other test groups (Figure – 3.16 and 3.17). Mice around this time seemed healthier in comparison to others with gained weight. Although reaching week 6 both tumor burden and volume increased significantly even more so than the control group. Survival was the same as control animals.

3.3.6) MRI Protocol Optimization

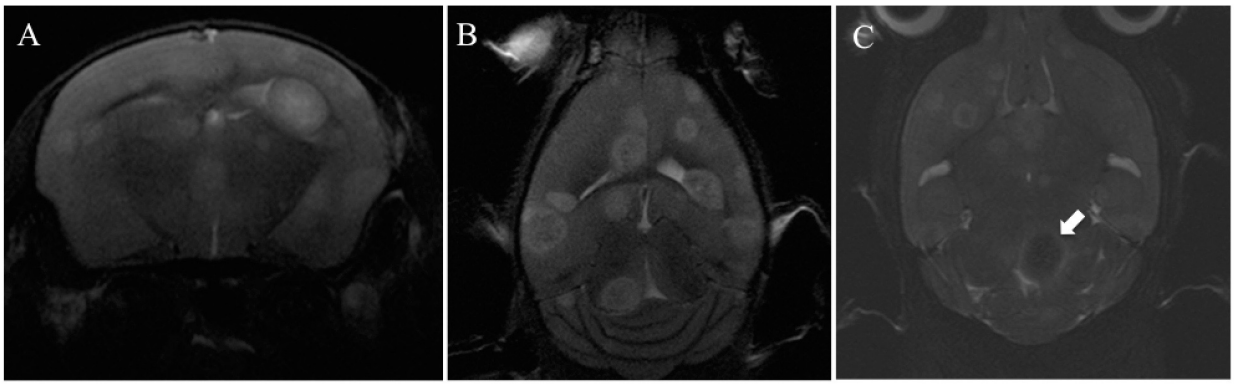

Figure 3.20 – Representative MRI Scans showing progress of MRI protocol optimization. A – Axial T1 weighted scan with 1mm thickness. B – Coronal T1 weighted scan with contrast with 0.5mm thickness. C – Coronal T2 weighted scan with contrast, with black spot (Contrast leaking from blood vessels; white arrow).

During the pilot study (TSA study) it was often difficult to see the tumors on T1 weighted images in axial sections with a slice thickness of 1 mm (Fig A). Unsatisfied with the results we wanted to test coronal slice selection instead (Fig B). Further, to improve resolution, we used 0.5mm slice thickness instead and increased Number of Averages. By doing coronal+0.5mm it was a lot easier to see the tumors, compared to axial. Further, we performed a T2 weighted scan after administering contrast and then the T1 sequence. The reason is: If the blood brain barrier is leaky, Omniscan will leak out from the blood vessels and accumulate in the tumor tissue. When a T2w scan is performed, the Omniscan contrast will then affect the contrast in this area. Omniscan will result in larger inhomogeneities in the tumor tissue, and transverse relaxation is lost much quicker than without Omniscan (so the T1 contrast agent has in fact a T2 effect as well). As a result the leaky tumors will appear as hypointensive (i.e. black) spots (Fig. C).

4) Discussion/Conclusion

In general, 40-60% of all cancer patients develop brain metastases during the progression of malignancy, of which a fifth are diagnosed with secondary brain tumors before the primary site neoplasm is located or identified **(**44). The current treatments are not effective, so it is of uttermost importance to find alternative treatment strategies. Chemotherapy alone is generally ineffective for the treatment of melanoma CNS metastases. Failure of systemic treatment for brain metastases in the past has been blamed on the inability of most experimental agents to pass the blood–brain barrier in addition to the low activity of these agents against melanoma (18, 45). An alternative would be to investigate and study other compounds, but the development of a new drug is risky and an expensive process (46). It takes on average 12 years and over US$350 million to get a new drug from the laboratory onto the pharmacy shelf. Once a company develops a drug, it undergoes around three and a half years of laboratory testing, before an application is made to the U.S. Food and Drug Administration (FDA) to begin testing the drug in humans. Only one in 1000 of the compounds that enter laboratory testing will ever make it to human testing. (47).

A different approach to this issue is the main objective of this work, which is to re-purpose drugs, which are already FDA approved, to cut the waiting period.

In a previous work, a list of genes potentially important in metastasis to the brain was identified. Through the capabilities of cMAP, a list of 20 compounds were published and resulted in the exact opposite gene profile. Ten of these compounds had already been tested; the objective of this work was to screen the remaining (chapter 2.1).
In this project a variety of *in vitro screening* assays were performed to study the effect of the selected drugs on four human metastatic melanoma cell lines. The most promising of these drugs were then tested in an *in vivo* model system.

All drugs were subjected to Monolayer Proliferation assay on all four human melanoma metastatic cell lines; in this assay 4 drugs were excluded (Sulphapyridine, Decamethonium Bromide, Fluticasone and Gabexate). These drugs showed no potential inhibition on cell proliferation therefore were not subjected to Soft Agar Assay. The promising drugs were Trichostatin A, Lanatoside C, Pentamidine, Methyldopa and Lymecycline. Trichostatin A is a potent histone deacetylase inhibitor that has proven effective against breast cancer both *in vitro* and *in vivo*, resulting in cell apoptosis **(**48, 49). Lanatoside C has been proven to upregulate the death receptor 5 inducing apoptosis through a caspase

independent cell death pathway (50). Pentamidine inhibits PRL family of oncogenic phosphatases, which potentially have a pathogenic role in human malignancies. It was tested on human WM9 melanoma cells and growth inhibition and necrosis was observed (51). Lymecycline is a tetracycline antibiotic that inhibits cell growth by inhibiting translation. This results in inhibition of protein synthesis and hence cell growth (52). No information relative to pathway of action of Methyldopa has been specified, but it is a very cytotoxic drug, and concentration administered and direct cell contact is probably the reason cell growth was affected (53).

Soft Agar analysis with the 5 effective drugs from the Monolayer Proliferation assay also showed promising inhibitional properties on all cell lines. The most promising drugs following these experiments were Trichostatin A and Lanatoside C, having consistent results in all cell lines with IC_{50} values in the (10^{-7}) range.

Due to the limited period of stay at UoB, Norway (Erasmus Period) and after careful deliberation it was decided to use one of these drugs in an *in vivo* pilot study. Trichostatin A was the selected drug, due to results in preliminary *in vitro* screening and because of its molecular weight of 302,37 Da, ideal to cross the BBB see chapter 1.6. Trichostatin A is an antifungal antibiotic that selectively inhibits mammalian histone deacetylases class I and II, and it is a potential chemotherapeutic agent (48) which has never been tested on melanoma brain metastasis. *In vivo* results using this drug differed from what was expected after *in vitro* screening. MRI scans were performed on weeks 4, 6 and 8 of the experiment, and it was clearly observed that animals treated with TSA had tumors higher in number and volume compared to untreated animals **(figure. – 3.11)**. Weekly weighing was performed to certify the animal's wellbeing, treated animals kept their weight more than control animals.

Due to the limitations of the BBB, Lymecycline and Lanatoside C were excluded from the following experiments (Cell cycle analysis and apoptosis) and therefore the remaining drugs to be tested were Methyldopa and Pentamidine. Cell cycle Analysis was performed of all cell lines with a concentration of 100mM of each drug and a respective positive and negative control. Results where not coherent between cell lines but shifts were observed in all cases. In general when treated with Methyldopa we notice a broadened G_2/M phase with the exception of Melmet 5 where we verified a broadened G_1 and S phase. The G_2/M DNA damage checkpoint consists of an arrest of the cell in G_2 just before mitotic entry in response to genotoxic stress (54). The arrest caused by Methyldopa exposure, could be associated in

part, with inhibited activity of p34(cdc2) kinase and reduced accumulation of p34 (cdc2) and cyclin B1 proteins (55). In cancer, G_1 phase is affected, generally because gene regulatory proteins of the E2F family have become unrestrained and G_1/S cyclin gene expression is increased, leading to uncontrolled cell-cycle entry (56). Methyldopa may be preventing cells from entering G_1 phase, therefore stopping Melmet 5 cells from dividing and spreading.

When treating H1_DL2 and Melmet 1 cells with Pentamidine, we verified a shift in G_1 phase; there was an accumulation of cells in the first and a reduction in the latter. In H1_DL2 it seems that cells cannot transition into the next phase and in Melmet 1 they cannot enter G_1 phase. H3 and Melmet 5 have a rise in the G_2/M phase, same as described above. So we can conclude that the drugs did affect the cell cycle at some point.

Both drugs were subjected to an apoptosis assay, to quantify apoptotic content through the aid of flow cytometry. Very coherent and statistically relevant data ($P \leq 0.0001$) resulted from cell exposure to drug concentration of 100mM. Cell apoptosis was in the range of 95-99%. A possible explanation could be p38 activation as well as ERK and Akt inactivation, which will result in apoptosis (57). We did not have time to perform Western Blot in order to confirm this.

Up to now Methyldopa and Pentamidine proved to be very strong candidates so they were subjected to an *in vivo* study as described above, see 3.3.3. MRI scans were performed on week 4 and 6 to verify and quantify tumor burden and volume. Results with Pentamidine were very similar to untreated animals, and no tumor effects could be seen. In contrast, when treated with Methyldopa, on week 4 the results looked promising with a reduction in tumor number and volume **(Fig. - 3.16),** which was also visible in the animals weights **(Fig. – 3.19)**, and around day 28 animals gained weight and had a healthier appearance. Unfortunately the animal's heath rapidly depleted around week 6, where tumor burden and volume grew to same levels observed both in the untreated mice and in the mice treated with Pentamidine.

Nonetheless, Methyldopa had a transient effect around week 4, which could mean that this drug should not be discarded as a possible form of treatment. This was not the case for week 6, but by optimizing protocol and maybe combining it with other drugs, it may still have a value. Professor Thorsen's group has showed treatment effects using **β**-sitosterol, and combined treatment with Methyldopa should be an aim for further studies. Therefore, further

studies still need to be performed, in the hope that this drug could also be trialed, as preventive form of treatment to melanoma brain metastasis.
It is also possible that results could be different for all drugs verified *in vivo* if other concentrations and drug delivery methods were tested. TSA has been tested *in vivo* before and administration was performed subcutaneously. (48).

In addition, because MRI protocols were optimized, it is now easier to detect the tumors, especially the smaller ones. In addition it is also possible to verify whether the tumors are leaky or not. This could be used in future animal studies, to see whether leakiness changes as a function of treatment.

5) Future aspects

Further studies should be performed to verify the applicability of Methyldopa in the treatment of melanoma metastasis. *In vivo* studies should be performed experimenting with different doses and forms of administration. Furthermore, results from this work suggest that Methyldopa could be applied as a preventive form of treatment, and this should also be tested by starting treatment for instance one week before tumor cell injections.

Lanatoside C showed very good results *in vitro* and should not be discarded; its main obstacle is the BBB. Once there is a way to open and facilitate the passage through the BBB, this drug should be an immediate candidate. Work is now ongoing in Thorsens lab, to transiently open the BBB by using a novel K16ApoE peptide (58). The group is able to effectively permeabilise the BBB, as shown by MRI, and future studies will aim at delivering therapeutic compounds that are not able to penetrate through intact brain vessels.

Additionally all these proposed studies will require *in vivo* studies, and utilizing the optimized MRI protocol will be of great benefit, since improved resolution and the ability to study tumor leakiness will add further value to the studies.

6) References

1) Stewart B, Wild C. (2014) *World Cancer report*. World Health Organization

2) Sadava, David E. *Life, The Science Of Biology*. Sunderland, MA: Sinauer Associates, 2008.

3) Hanahan D, Weinberg RA. 2011. Hallmarks of cancer: the next generation. *Cell.***144**:646-674.

4) Chen DS, Mellman I. 2013. Oncology meets immunology: the cancer-immunity cycle. *Immunity*. **39**:1-10.

5) Mellman I, Coukos G, Dranoff G. 2011. Cancer immunotherapy comes of age. *Nature.* **480**:480-489

6) Hirohashi S. 1998. Inactivation of the E-cadherin-mediated cell adhesion system in human cancers. *American Journal of Pathology*. **153**: 333–339

7) Jo M, Lester RD, Montel V, Eastman B, Takimoto S, Gonias SL. 2009. Reversibility of epithelial–mesenchymal transition (EMT) induced in breast cancer cells by activation of urokinase receptor-dependent cell signaling. *Journal of Biological Chemistry*. **284**: 22825–22833

8) Cano A, Perez-Moreno MA, Rodrigo I, Locascio A, Blanco MJ, del Barrio MG, Portillo F, Nieto MA. 2000. The transcription factor snail controls epithelial–mesenchymal transitions by repressing E-cadherin expression. *Nature Cell Biology*. **2**: 76–83.

9) Tsai J and Yang J. 2013. Epithelial - mesenchymal plasticity in carcinoma metastasis. *Genes and Development*. **27**: 2192-2206

10) Venkitaraman AR. 2001. Functions of BRCA1 and BRCA2 in the biological response to DNA damage. *Journal of Cell Science*. **114**:3591-3598.

11)Alberts B, Johnson A, Lewis J, et al. Molecular Biology of the Cell. 4th edition. 2002, New York: Garland Science.

12) http://cyberbridge.mcb.harvard.edu/mitosis_3.html

13) Andreeff M GD, Pardee AB. 2003. Cell proliferation and differentiation. Holland-Frei Cancer Medicine. Hamilton: BC Decker.

14) Ferlay J, Soerjomataram I, Ervik M, et al. GLOBOCAN 2012 v1.0, Cancer Incidence and Mortality Worldwide: IARC CancerBase No. 11. Lyon, France: International Agency for Research on Cancer; 2013

15)Ferlay J, Steliarova-Foucher E, Lortet-Tieulent J, et al. 2013. Cancer incidence and mortality patterns in Europe: Estimates for 40 countries in 2012. *European Journal of Cancer*. **49**: 1374-1403.

16)http://www.cancerresearchuk.org/about-cancer/type/skin-cancer/about/skin-cancer-risks-and-causes#quick

17)Chin L, Garraway L, Fisher D. 2006. Malignant melanoma: genetics and therapeutics in the genomic era. *Genes and Development*. **20**: 2149-2182

18)Thorsen F, Fite B, Mahakian LM, Seo JW, Qin S, Harrison V, Johnson S, Ingham E, Caskey C, Sundstrøm T, Meade TJ, Harter PN, Skaftnesmo KO, Ferrara KW. 2013. Multimodal imaging enables early detection and characterization of changes in tumor permeability of brain metastases. *Journal of controlled release: official journal of the Controlled Release Society*. **172(3)**: 812-822.

19) Mayer M. 2007. A patient perspective on brain metastases in breast cancer. *Clinical cancer research : an official journal of the American Association for Cancer Research*. **13(6)**: 1623-4

20) Fife KM, Colman MH, Stevens GN, Firth IC, Moon D, Shannon KF, Harman R, Petersen-Schaefer K, Zacest AC, Besser M, Milton GW, McCarthy WH, Thompson JF. Determinants of outcome in melanoma patients with cerebral metastases. Journal of clinical oncology : official journal of the American Society of Clinical Oncology. 2004;22(7):1293-300

21) Davies MA, Liu P, McIntyre S, Kim KB, Papadopoulos N, Hwu WJ, Hwu P, Bedikian A. Prognostic factors for survival in melanoma patients with brain metastases. Cancer. 2011;117(8):1687-96

22) Fidler I, Schackert G, Zhang R-d, Radinsky R, Fujimaki T. 1999 The Biology of Melanoma Brain Metastasis. *Cancer and Metastasis Reviews*. **18(3)**: 387-400.

23) Patchell RA, Tibbs PA, Walsh JW, Dempsey RJ, Maruyama Y, Kryscio RJ, Markesbery WR, Macdonald JS, Young B. 1990. A Randomized Trial of Surgery in the Treatment of Single Metastases to the Brain. *New England Journal of Medicine*. **322(8)**: 494-500

24) McWilliams RR, Rao RD, Buckner JC, Link MJ, Markovic S, Brown PD. 2008. Melanoma-induced brain metastases. *ExpertRev. Anticancer Ther*. **8(5)**: 743–755.

25) Knisely JPS, Yu JB, Flanigan J, Sznol M, Kluger HM, Chiang VL. 2012. Radiosurgery for melanoma brain metastases in the ipilimumab era and the possibility of longer survival. *Journal of Neurosurgery*. **117(2)**: 227–233

26) Majer M, Jensen RL, Shrieve DC *et al*. 2007. Biochemotherapy of metastatic melanoma in patients with or without recently diagnosed brain metastases. *Cancer*. **110(6)**: 1329–1337.

27) Quirt I, Verma S, Petrella T, Bak K, Charette M. 2007. Temozolomide for the treatment of metastatic melanoma: a systematic review. *Oncologist.* **12(9)**: 1114–1123.

28) Brightman MW. 1977. Morphology of blood-brain interfaces. *Experimental eye research.* 25 Suppl: 1-25.

29) Ohtsuki S, Hori S, Terasaki T. 2003. Molecular mechanisms of drug influx and efflux transport at the blood-brain barrier. *Nihon yakurigaku zasshi Folia pharmacologica Japonica*. **122(1)**: 55-64.

30) Lorger M, Felding-Habermann B. 2010. Capturing changes in the brain microenvironment during initial steps of breast cancer brain metastasis. The *American journal of pathology*. **176(6)**: 2958-71.

31) Laterra J KR, Betz LA, et al. 1999. Blood-brain barrier. In: Siegel GJ AB, Albers RW, et al. *Basic Neurochemistry*: Molecular, cellular and Medical aspects 6th edition.

32) Abbott NJ. 2002. Astrocyte-endothelial interactions and blood-brain barrier permeability. *Journal of anatomy*. **200(6)**: 629-38.

33) Purves D AG, Fitzpatrick D, et al. 2001. The Blood Supply of the Brain and Spinal Cord. Neuroscience 2nd edition.

34) Motl S, Zhuang Y, Waters CM, Stewart CF. 2006. Pharmacokinetic considerations in the treatment of CNS tumours. *Clinical pharmacokinetics*. **45(9)**: 871-903

35) Gabos Z, Sinha R, Hanson J, Chauhan N, Hugh J, Mackey JR, Abdulkarim B. 2006. Prognostic significance of human epidermal growth factor receptor positivity for the development of brain metastasis after newly diagnosed breast cancer. *Journal of clinical oncology: official journal of the American Society of Clinical Oncology*. **24(36)**: 5658-63

36) Vasiliou V, Vasiliou K, Nebert DW. 2009. Human ATP-binding cassette (ABC) transporter family. *Human genomics*. **3(3)**: 281-90

37) Zhang C, Yu D. 2011. Microenvironment determinants of brain metastasis. *Cell & bioscience*. **1(1)**: 8

38) Schinkel AH. 1999. P-Glycoprotein, a gatekeeper in the blood-brain barrier. Advanced drug delivery reviews. **36(2-3)**: 179-94.

39) Pozarowski P, Darzynkiewicz Z. 2004. Analysis of cell cycle by flow cytometry. *Methods in molecular biology*. **281**: 301-11.

40) Gray JW, Dolbeare F, Pallavicini MG, Beisker W, Waldman F, Division BS, Livermore L. 1986. Cell cycle analysis using flow cytometry. *International journal of radiation biology & related studies in physics chemistry & medicine* **49(2)**: 237-55.

41) Garber, Janet. GUIDEFOR THE CARE AND USE OF LABORATORY ANIMALS. Washinton DC: THE NATIONAL ACADEMIES PRESS, 2011

42) Currie S, Hoggard N, Craven IJ, Hadjivassiliou M, Wilkinson ID. 2013. Understanding MRI: basic MR physics for physicians. *Postgraduate medical journal*. **89(1050)**: 209-23

43) Pooley RA. 2005. AAPM/RSNA Physics Tutorial for Residents - Fundamental Physics of MR Imaging. *RadioGraphics*. **25:**1087-99.

44) Campos S, Davey P, Hird A, Pressnail B, Bilbao J, Aviv RI, et al. 2009. Brain metastasis from an unknown primary, or primary brain tumour? A diagnostic dilemma. CURRENT ONCOLOGY. **16(1)**: 5.

45) Quirt I, Verma S, Petrella T, Bak K, Charette M. 2007. Temozolomide for the treatment of metastatic melanoma: a systematic review. *Oncologist.* **12(9)**: 1114–1123.

46) DiMasi JA. 2001. Risks in new drug development: approval success rates for investigational drugs. *Clinical Pharmacological Therapy*. **69**: 297-307

47) http://www.drugs.com/fda-approval-process.html

48) Vigushin D, Ali S, Pace P, Mirsaidi N, Ito K, Adcock I, Coombes R. 2001. Trichostatin A Is a Histone Deacetylase Inhibitor with Potent Antitumor Activity against Breast Cancer *in Vivo*. *Clinical Cancer Research.* **7**: 971.

49) Tavakoli-Yaraki M, Karami-Tehrani F, Salimi V, Sirati-Sabet M. 2013 Induction of apoptosis by Trichostatin A in human breast cancer cell lines: involvement of 15-Lox-1. *Tumour Biol.* **34(1)**: 241-9

50) Badr C, Wurdinger T, Nilsson J, Niers J, Whalen M, Degterev A and Tannous B. 2011. Lanatoside C sensitizes glioblastoma cells to tumor necrosis factor-related apoptosis-inducing ligand and induces an alternative cell death pathway. *Neuro Oncology*. **13(11)**: 1213-1224

51) Pathak M, Dhawan D, Lindner D, Borden E, Farver C, Yi T. 2002. Pentamidine is an inhibitor of PRL phosphatases with anticancer activity. *Mol Cancer Ther.* **1(14)**:1255-64

52) Song, K.S. (2004). Ribosomal protein synthesis inhibitors. In S. Offermanns, & W. Rosenthal. *Encyclopedic reference of molecular pharmacology* (pp. 827-833).

53) http://www.inchem.org/documents/pims/pharm/methyldo.htm#SectionTitle:7.1%20Mode%20of%20action

54) Taylor, W. R.; Stark, G. R. 2001. Regulation of the G2/M transition by p53. *Oncogene* **20(15)**: 1803–1815

55) Wang W, Heideman L, Chung CS, Pelling JC, Koehler KJ, Birt DF. 2000. Cell-cycle arrest at G2/M and growth inhibition by apigenin in human colon carcinoma cell lines. *Molecular carcinogenesis.* **(2)**: 102-10

56) Morgan, David. The Cell Cycle: Principals of Control. London: New Science Press LTD, 2007

57) Ye Y, Wang H, Chu J, Chou G, Chen S, Mo H, Fong W and Yu Z. 2011. Atractylenolide II induces G1 cell-cycle arrest and apoptosis in B16 melanoma cells. *Journal of Ethnopharmacology*. **136(1)**: 279 – 282.

58) Sarkar G, Curran GL, Sarkaria JN, Lowe VJ, Jenkins RB. 2014. Peptide Carrier-Mediated Non-Covalent Delivery of Unmodified Cisplatin, Methotrexate and Other Agents via Intravenous Route to the Brain. *PLoS ONE*. **9(5)**: e97655.